© 2020. Published by The Company of Biologists Ltd | Journal of Cell Science (2020) 133, jcs243840. doi:10.1242/jcs.243840

RESEARCH ARTICLE

LDL uptake-dependent phosphatidylethanolamine translocation to the cell surface promotes fusion of osteoclast-like cells

Victor J. F. Kitano[1,2], Yoko Ohyama[1,2], Chiyomi Hayashida[1], Junta Ito[3], Mari Okayasu[4], Takuya Sato[1], Toru Ogasawara[4], Maki Tsujita[5], Akemi Kakino[6], Jun Shimada[2], Tatsuya Sawamura[6] and Yoshiyuki Hakeda[1,*]

ABSTRACT

Osteoporosis is associated with vessel diseases attributed to hyperlipidemia, and bone resorption by multinucleated osteoclasts is related to lipid metabolism. In this study, we generated low-density lipoprotein receptor (*LDLR*)/lectin-like oxidized LDL receptor-1 (*LOX-1*, also known as *Olr1*) double knockout (dKO) mice. We found that, like *LDLR* single KO (sKO), *LDLR*/*LOX-1* dKO impaired cell–cell fusion of osteoclast-like cells (OCLs). *LDLR*/*LOX-1* dKO and *LDLR* sKO preosteoclasts exhibited decreased uptake of LDL. The cell surface cholesterol levels of both *LDLR*/*LOX-1* dKO and *LDLR* sKO osteoclasts were lower than the levels of wild-type OCLs. Additionally, the amount of phosphatidylethanolamine (PE) on the cell surface was attenuated in *LDLR*/*LOX-1* dKO and *LDLR* sKO preosteoclasts, whereas the PE distribution in wild-type OCLs was concentrated on the filopodia in contact with neighboring cells. Abrogation of the ATP binding cassette G1 (ABCG1) transporter, which transfers PE to the cell surface, caused decreased PE translocation to the cell surface and subsequent cell–cell fusion. The findings of this study indicate the involvement of a novel cascade (LDLR∼ABCG1∼PE translocation to cell surface∼cell–cell fusion) in multinucleation of OCLs.

KEY WORDS: Osteoclast-like cells, Cell–cell fusion, Low-density lipoprotein receptor, Phosphatidylethanolamine, Cholesterol, ATP binding cassette G1 transporter

INTRODUCTION

Multinucleated osteoclasts are the cells responsible for physiological and pathological bone resorption and belong to the monocyte/macrophage cell lineage. Although many systemic hormones and local cytokines regulate osteoclast differentiation (Teitelbaum, 2007), the receptor activator of nuclear factor κB ligand (RANKL, also known as TNFSF11) and macrophage colony-stimulating factor (M-CSF, also known as CSF1) are essential cytokines in osteoclastogenesis (Yasuda et al., 1998). RANKL signals produced by bone marrow stromal cells or osteoblasts are introduced into osteoclast precursors via a receptor of RANKL (RANK, also known as TNFRSF11A) on the plasma membrane of osteoclast lineage cells, leading to the activation of nuclear factor κB (NF-κB) and MAPKs (Asagiri and Takayanagi, 2007; Mizukami et al., 2002). Activation of the signaling molecules then induces the expression of NFATc1 (Takayanagi et al., 2002), a master transcription factor for osteoclast differentiation. Therefore, the expression of osteoclast function-related molecules, including tartrate-resistant acid phosphatase (TRAP), cathepsin K and fusion-related proteins such as ATP6v0d2 and DC-STAMP, is induced (Inaoka et al., 1995; Lee et al., 2006; Kim et al., 2010; Yagi et al., 2005; Mensah et al., 2010).

Accumulating epidemiological evidence has demonstrated that dyslipidemia is a risk factor not only for atherosclerosis and vascular calcification but also for osteoporosis, indicating a tight correlation between skeletal homeostasis and lipid metabolism (Pinals and Jabbs, 1972; Banks et al., 1994; Yamaguchi et al., 2002; Alagiakrishnan et al., 2003). We have thus far demonstrated that differentiation of osteoclast-like cells (OCLs) is impacted by the status of intracellular and extracellular low-density lipoprotein (LDL) or cholesterol (Hada et al., 2012; Okayasu et al., 2012). Caveolin-1, a principal scaffolding protein of cholesterol and sphingolipid-enriched flask-shaped caveolae and lipid rafts in the plasma membrane, expression in OCLs was induced by RANKL signaling during osteoclastogenesis, and the removal of cholesterol from the plasma membrane caused abnormal signaling for osteoclastogenesis (Hada et al., 2012). Furthermore, the abrogation of LDL receptor (LDLR) impaired OCL formation because of defects in cell–cell fusion of OCLs; thereby, the trabecular bone mass was increased, indicating that uptake of LDL is required for osteoclastogenesis (Okayasu et al., 2012). On the other hand, lectin-like oxidized LDL receptor-1 (LOX-1, also known as OLR1) recognizes extracellular oxidized LDL and is crucially involved in the pathogenesis of atherosclerosis, a multifactorial inflammatory disease of the vessel wall that can cause heart disease and stroke (Yoshimoto et al., 2011). The deletion of LOX-1 promoted OCL formation as a result of increased cell–cell fusion, thereby decreasing bone volume (Nakayachi et al., 2015). Although LDLR and LOX-1 oppositely affect OCL cell–cell fusion, neither receptor affects the expression of osteoclast differentiation molecules, such as NFATc1 and cathepsin K (Nakayachi et al., 2015). These results indicate that LDLR and LOX-1 modulate OCL cell–cell fusion through a cascade other than the well-known osteoclast differentiation signaling pathway via the RANKL/RANK complex. However, the molecular mechanism underlying the actions of LDLR and LOX-1 on cell–cell fusion remains unknown.

It has been recently demonstrated that dynamic translocation of phospholipids, principally phosphatidylethanolamine (PE) and phosphatidylserine (PS), from the inner to outer leaflet of the

[1]Division of Oral Anatomy, Meikai University School of Dentistry, Sakado, Saitama 350-0283, Japan. [2]Division of Oral and Maxillofacial Surgery, Meikai University School of Dentistry, Sakado, Saitama 350-0283, Japan. [3]Josai University, Faculty of Pharmacy and Pharmaceutical Sciences, Department of Clinical Dietetics and Human Nutrition, Sakado, Saitama 350-0295, Japan. [4]Division of Oral-maxillofacial Surgery, Dentistry and Orthodontics, The University of Tokyo Hospital, Hongo, Tokyo 113-8655, Japan. [5]Department of Biochemistry, Graduate School of Medical Sciences, Nagoya City University, Kawasumi, Mizuho-cho, Mizuho-ku, Nagoya, Aichi 467-8601, Japan. [6]Department of Physiology, Shinshu University School of Medicine, Matsumoto, Nagano 390-8621, Japan.

*Author for correspondence (y-hakeda@dent.meikai.ac.jp)

V.J.F.K., 0000-0003-4001-5701; M.T., 0000-0003-1108-621X; A.K., 0000-0002-9612-4256; T.S., 0000-0002-5415-2080; Y.H., 0000-0001-7233-2600

Handling Editor: John Heath
Received 14 January 2020; Accepted 25 March 2020

Journal of Cell Science (2020) 133, jcs243840. doi:10.1242/jcs.243840

plasma membrane plays an important role in cell–cell fusion during OCL maturation (Irie et al., 2017; Verma et al., 2018). Cell–cell fusion is a fundamental physiological event for egg–sperm fusion for fertilization and for the generation of multinucleated placental syncytiotrophoblasts, myogenesis and osteoclastogenesis (Oren-Suissa and Podbilewicz, 2007; Xing et al., 2012); moreover, cell–cell fusion is involved in the pathological formation of macrophage foreign body giant cells (Xing et al., 2012). Cell–cell fusion occurs in several steps. First, cells recognize partner cells and then the outer leaflets of the plasma membrane of the two cells come into contact with each other. This is followed by formation of a hemifusion stalk and a hemifusion diaphragm. Finally, a fusion pore is generated to complete cell–cell fusion (Chernomordik and Kozlov, 2008). During the cell–cell fusion process, dynamic changes in the distribution of phospholipids, the principal components of membrane bilayers, occur between the outer and inner leaflets of the membrane. The kinetic alteration (flip-flop) is mediated by three different types of enzymes (Montigny et al., 2016): flippases that mediate the transport of phospholipids from the outer to inner leaflet of the plasma membrane, floppases that arbitrate migration from the inner to outer leaflet and scramblases that catalyze the bidirectional distribution change of phospholipids. Flippases, floppases and scramblases include the P-type ATPase superfamily (Zhou and Graham, 2009), ATP binding cassette (ABC) transporters (Hankins et al., 2015) and anoctamin/TMEM16 family (Suzuki et al., 2010), respectively.

To explore the molecular mechanism underlying the effects of LDLR and LOX-1 on cell–cell fusion of OCLs, we used *LDLR* single KO (sKO), *LOX-1* sKO and *LDLR/LOX-1* double KO (dKO) mice in this study. We found that translocation of PE to the outer leaflet of the plasma membrane from the inner leaflet is pivotally dependent on LDL uptake through LDLR and that the translocation mediated by the ATP binding cassette G1 (ABCG1) transporter is required for the cell–cell fusion of OCLs. These results provide novel insight into the mechanism of osteoclast cell–cell fusion.

RESULTS

In vitro OCL formation from *LDLR*/*LOX-1* dKO monocytes treated with M-CSF and sRANKL

We generated *LDLR/LOX-1* dKO mice by cross-mating *LDLR* sKO and *LOX-1* sKO mice. Using *LDLR/LOX-1* dKO mice, we first examined the effect of abrogation of both *LDLR* and *LOX-1* genes on *in vitro* OCL formation in response to M-CSF and sRANKL (Fig. 1A). The number of TRAP-positive multinucleated OCLs with more than three nuclei in the culture of *LDLR/LOX-1* dKO monocytes treated with M-CSF and sRANKL was equivalent to that in the culture of wild-type (WT) cells (Fig. 1B, left panel). However, the area of *LDLR/LOX-1* dKO multinucleated OCLs was decreased by approximately 20% of the area of WT osteoclasts (Fig. 1B, middle panel). Consistent with the decreased area of OCLs, the fusion index, which was expressed as the mean number of nuclei per multinucleated OCL, in the cultures of *LDLR/LOX-1* dKO monocytes was also reduced to approximately 25% of that of WT cells (Fig. 1B, right panel). Because the fusion index indicates the frequency of cell fusion to form multinucleated OCLs, the decreased fusion index indicated that the cell–cell fusion of mononuclear preosteoclasts (pre-OCLs) into mature multinucleated OCLs was impaired by the deletion of both *LDLR* and *LOX-1* genes. The reduction in cell–cell fusion is consistent with the decrease in cell–cell fusion as a result of *LDLR* single deletion (Okayasu et al., 2012); this finding suggests that LDLR is required for cell–cell fusion of OCLs. However, the mRNA levels of osteoclast differentiation-related molecules, such as c-Fos, NFATc1, TRAP and cathepsin K, and fusion-related proteins, including DC-STAMP, OC-STAMP and ATP6v0d2, in *LDLR/LOX-1* dKO osteoclastic cells were not altered compared with the mRNA levels in WT OCLs (Fig. S1).

Uptake of LDL, accumulation of neutral lipids (including cholesterol) and cell surface cholesterol distribution of pre-OCLs

To address the role of LDLR in osteoclastogenesis, we next compared the uptake of LDL into the cells using four different

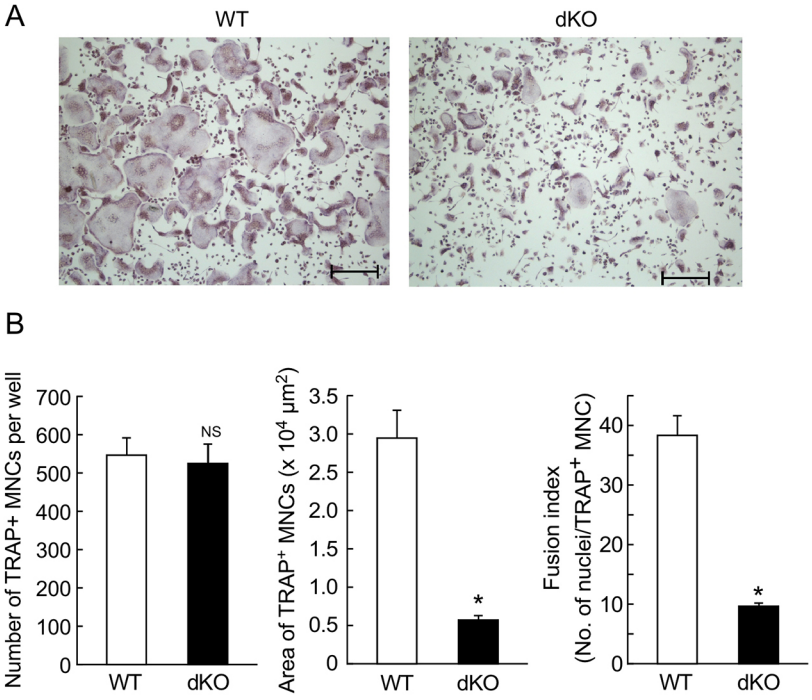

Fig. 1. *In vitro* osteoclastogenesis from *LDLR1*/*LOX-1* double knockout OCL precursors. OCL precursors from WT and *LDLR1*/*LOX-1* dKO bone marrow cells were cultured with sRANKL (10 ng/ml) and M-CSF (20 ng/ml) for 2.5 days. After culturing, the cells were stained for TRAP activity. (A) Photographs of TRAP-positive OCLs formed in the cultures. (B) Left: The number of TRAP-positive MNCs with ≥3 nuclei was measured (n=4). Experiments were performed in triplicate and reproducibility confirmed. Values represent the mean±s.d. Middle and right: More than 100 TRAP-positive multinucleated cells (MNCs) in each culture were randomly selected and the average area of the formed TRAP-positive MNCs measured. The fusion index is presented as the average number of nuclei per TRAP-positive MNC that was formed in the culture (n≥100 cells per culture). Values represent the mean±s.e.m. *P<0.05 versus culture derived from WT mice. NS, not significant. Scale bars: 250 µm.

Journal of Cell Science (2020) 133, jcs243840. doi:10.1242/jcs.243840

genotypes of OCLs: WT, *LDLR/LOX-1* dKO, *LOX-1* sKO and *LDLR* sKO (Fig. S2A). The OCLs were incubated with pHrodo Red-labeled LDL following starvation of extracellular and intracellular LDL in the serum. An obvious red-color signal indicating the uptake of exogenous LDL was observed in WT OCLs. Although LDL uptake into *LOX-1* sKO OCLs was lower than that of WT OCLs, significant uptake was confirmed. In contrast, the uptake of LDL into *LDLR* sKO and *LDLR/LOX-1* dKO OCLs was small, indicating that the LDL uptake of OCLs is dependent on the presence of LDLR.

Furthermore, neutral lipids, including cholesterol, that are stained with Oil Red O solution were evidently accumulated in WT and *LOX-1* sKO OCLs (Fig. S2B). In contrast, such accumulation was not observed in *LDLR/LOX-1* dKO and *LDLR* sKO OCLs.

Next, we determined the amount of cell surface cholesterol using cell membrane-impermeable *θ*-toxin-derived domain 4 (D4), which specifically binds cholesterol (Shimada et al., 2002). Cholesterol was abundant on the cell surface of WT and *LOX-1* sKO OCLs, and the amount of cholesterol was abolished by pretreatment with methyl-β-cyclodextrin (MβCD), which binds and removes cholesterol from the outer leaflet of the plasma membrane (Fig. 2A,B). The cell surface cholesterol level of *LDLR/LOX-1* dKO and *LDLR* sKO OCLs was faint, and the decreased amount was approximately 20% of that of WT and *LOX-1* sKO cells (Fig. 2B), suggesting that the status of intracellular cholesterol in OCLs is crucially determined by the level of LDLR.

LDLR/*LOX-1* dKO pre-OCLs exhibit a decrease in cell surface PE distribution

It has been recently reported that PE dynamics of the plasma membrane are required for cell–cell fusion of OCLs (Irie et al., 2017). Therefore, we next determined the PE distribution on the cell surface of WT and *LDLR/LOX-1* dKO OCLs using SA–biotin-conjugated Ro09-0198 (SA–Bio-Ro), which specifically binds PE (Choung et al., 1988). Because SA–Bio-Ro is cell membrane impermeable, the probe has been used for the detection of PE residing in the outer, but not inner, leaflet of the plasma membrane. However, in a variety of cells, PE is abundantly distributed in the inner leaflet of the plasma membrane (van Meer et al., 2008). Mononuclear WT pre-OCLs prior to maturation possessed numerous filopodia structures, which were connected to the filopodia of adjacent cells. Furthermore, PE was concentrated and restricted in the filopodia (Fig. S3A,B), indicating that PE accumulates on the surface of filopodia of pre-OCLs as a result of translocation of PE from the inner leaflet. In contrast, the distribution of cholesterol was ubiquitous on the whole cell surface.

PE translocation into the outer leaflet of the plasma membrane of WT OCLs occurred from the early stage of osteoclast differentiation, and as osteoclast multinucleation proceeded, the cell surface PE level gradually decreased (Fig. 3A-C). In all cases, the cell surface PE level of *LDLR/LOX-1* dKO OCLs was significantly lower than that of WT OCLs (Fig. 3A-C).

Expression of ABC transporters in OCLs and the involvement of LDLR in PE translocation into the outer leaflet of the plasma membrane

The movement of lipid substrates, including various phospholipids and cholesterol from the inner to outer leaflets of the plasma membrane, is mediated by a variety of ABC transporters (Coleman et al., 2013). Irie et al. (2017) reported that ABCB4 and ABCG1 are required for cell–cell fusion of OCLs to the cell surface through PE dynamics. Thus, we examined the mRNA expression profile of the

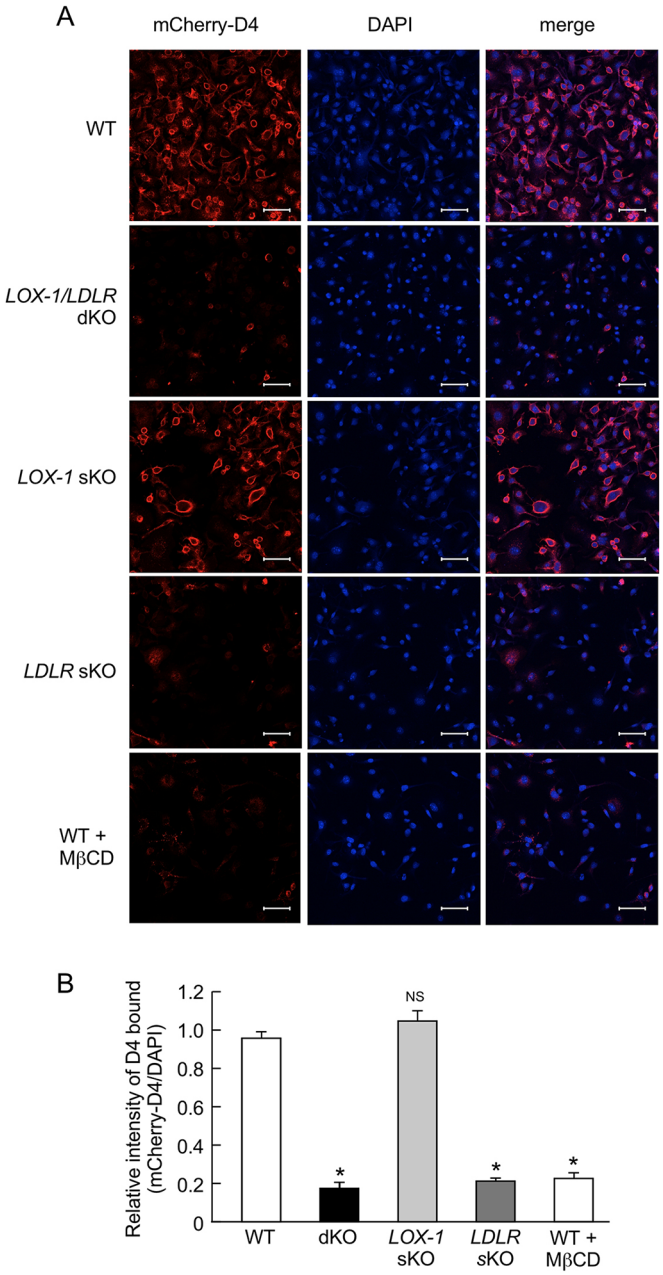

Fig. 2. Amount of cholesterol on the cell surface of OCLs. (A) OCL precursors from mice of four different genotypes (WT, *LDLR/LOX-1* dKO, *LOX-1* sKO and *LDLR* sKO) were cultured with M-CSF and sRANKL for 2 days. After culturing, the cells were incubated with His-tag-mCherry-D4 for 30 min and then fixed. The nuclei of the fixed cells were stained with DAPI. For the negative control, WT OCLs were pretreated with MβCD (10 mM) for 30 min prior to incubation with His-tag-mCherry-D4. (B) More than 100 cells were randomly selected and the relative immunofluorescence intensity of His-tag-mCherry-D4 on the cell surface calculated as per the intensity of DAPI in the cells. Experiments were performed in triplicate and reproducibility confirmed. Values represent the mean±s.e.m. **P*<0.05 versus culture of WT OCLs, NS not significant. Scale bars: 50 µm.

ABC transporters in four different types of genotypic OCLs. On day 1 after sRANKL addition, the level of *Abcg1* mRNA in WT OCLs was attenuated to approximately 70% of the level before addition of sRANKL; however, the reduced level was maintained at approximately 50-70% of the initial level during OCL formation (Fig. 4A). In *LDLR/LOX-1* dKO OCLs, the initial (on day 0)

Journal of Cell Science (2020) 133, jcs243840. doi:10.1242/jcs.243840

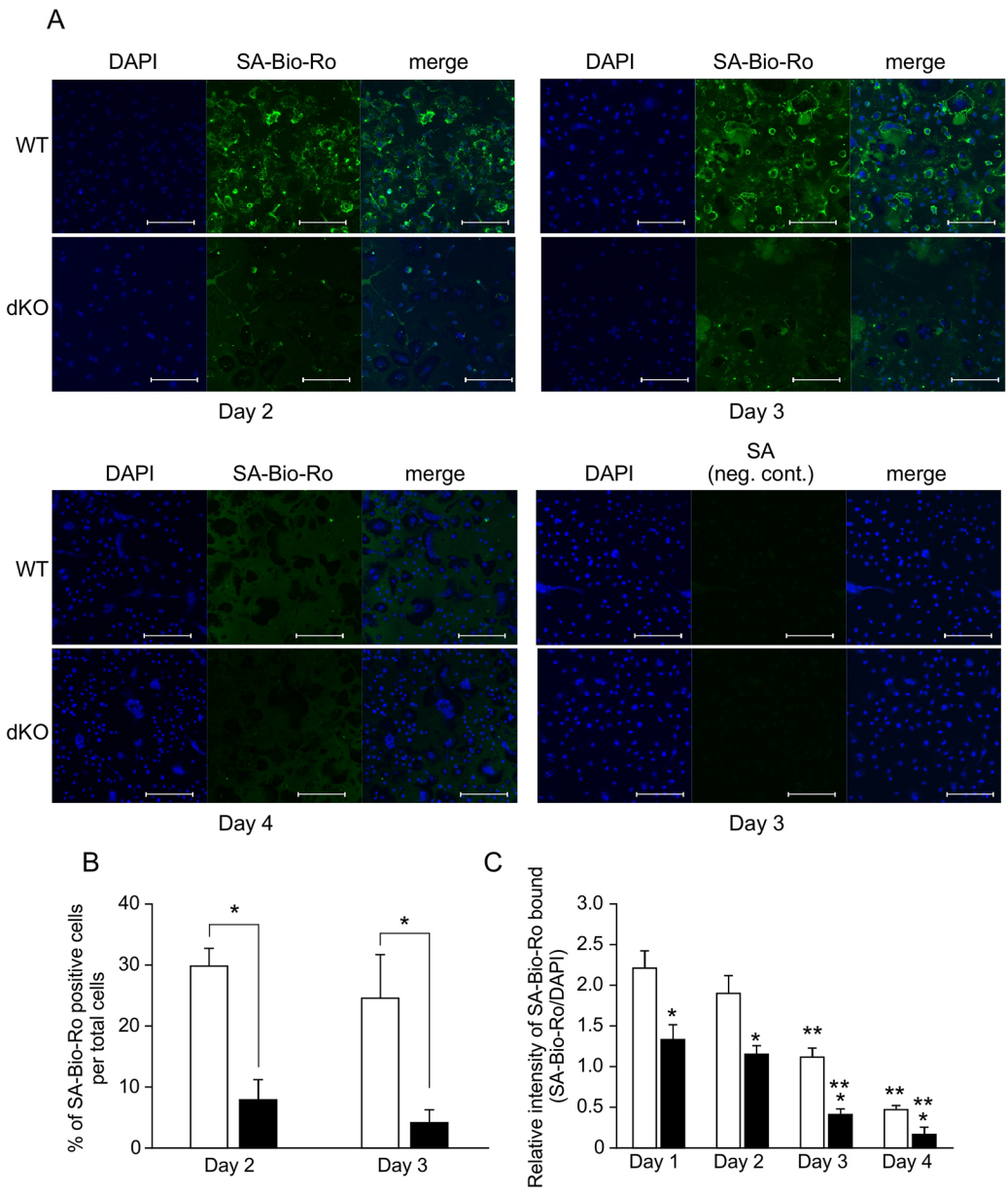

Fig. 3. Decreased PE distribution in the outer leaflet of the plasma membrane of *LDLR*/*LOX-1* dKO OCLs. (A) WT and *LDLR*/*LOX-1* dKO OCL precursors were cultured with M-CSF and sRANKL for the indicated number of days. After the culture, OCLs were stained with SA–Bio-Ro (green) and DAPI (blue) and were observed under a confocal laser microscope. (B) To quantify the level of PE in the outer leaflet of the plasma membrane of the cells, the percentage of cells positive for SA–Bio-Ro per randomly selected cell ($n \geq 100$) was determined. (C) The intensity of SA–Bio-Ro relative to the intensity of DAPI was also measured ($n \geq 25$). Experiments were performed in triplicate and reproducibility confirmed. Values represent the mean±s.e.m. *P<0.05 versus culture of WT osteoclastic cells on each day. **P<0.05 versus culture on day 1 in each OCL genotype. Scale bars: 100 µm.

expression level of *Abcg1* mRNA was approximately 60% lower than that of WT OCL precursors (Fig. 4A). The expression level was greatly reduced to approximately 1% of the initial level by day 1 of incubation with sRANKL, and the lower level was sustained throughout OCL formation (Fig. 4A). The difference in *Abcg1* mRNA levels between WT and *LDLR/LOX-1* dKO OCLs was significant during OCL differentiation. Although the *Abcg1* mRNA expression profile in *LOX-1* sKO OCLs was comparable to that of WT cells, the *Abcg1* mRNA level in *LDLR* sKO OCLs was severely decreased by sRANKL stimulation, consistent with the reduction in *LDLR/LOX-1* dKO OCLs (Fig. 4B). On the other hand, the *Abcb4* mRNA level was elevated with OCL differentiation, and the mRNA expression level in *LDLR/LOX-1* dKO OCLs was equivalent to that in WT OCLs (Fig. 4C). In addition, we recognized no significant difference in the *Abcb4* mRNA expression levels among WT, *LOX-1* sKO and *LDLR* sKO OCLs (Fig. 4D). In addition to ABCG1 and ABCB4, we also determined the mRNA levels of some other ABC transporters. During OCL differentiation, there was no significant difference in the mRNA expression profiles of ABCA1, ABCA2, ABCA3 and ABCB1β among the four different genotypic OCLs (Fig. S4). The expression of *Abca4* and *Abcg4* mRNAs was not detected in the OCLs. These results indicate that the large reduction in *Abcg1* mRNA expression in *LDLR/LOX-1* dKO and *LDLR* sKO OCLs coincides with the decrease in the cell–cell fusion of OCLs. Therefore, we again determined the PE level in the outer leaflet of the plasma membrane of *LDLR* sKO OCLs. We found that the PE level

Journal of Cell Science (2020) 133, jcs243840. doi:10.1242/jcs.243840

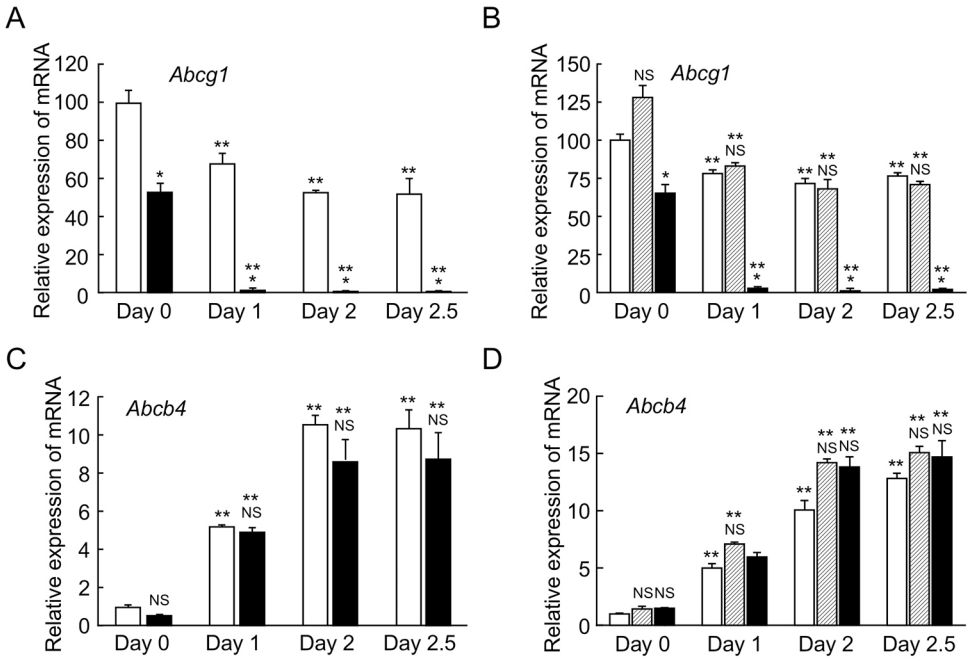

Fig. 4. Expression of *Abcg1* and *Abcb4* mRNA in WT and *LDLR/LOX-1* dKO OCLs during OCL differentiation. (A-D) OCL precursors from WT (open bars in A,C) and *LDLR/LOX-1* dKO (closed bars in A,C) mice were cultured with M-CSF and sRANKL for the indicated periods. In B,D, the open, hatched and closed bars indicate the values of WT, *LOX-1* sKO and *LDLR* sKO OCLs, respectively. After culture, total RNA was prepared and the synthesized cDNA subjected to quantitative real-time RT-PCR to determine the levels of *Abcg*1 mRNA (A,B) and *Abcb4* mRNA (C,D). Experiments were performed in triplicate and reproducibility confirmed. Values represent the mean±s.d. (n=3). *P<0.05 versus WT on each day. **P<0.05 versus culture on day 0 for each OCL genotype. NS, not significant between WT and each knockout culture on each day.

on the cell surface of *LDLR* sKO OCLs was markedly lower than that of WT cells, similar to the reduction in *LDLR/LOX-1* dKO cells (Fig. 5).

Decreased cell–cell fusion in *Abcg1* gene knockdown and knockout OCLs

Based on the above findings, we next examined the effect of *Abcg1* and *Abcb4* gene knockdown on OCL formation and cell–cell fusion by means of siRNA transduction. Electroporation of *Abcg1* siRNA decreased the expression level of *Abcg1* mRNA in WT OCLs to less than 10% compared with scramble RNA transduction, whereas the mRNA levels of *Abcb4* were not altered (Fig. 6A). In contrast, *Abcb4* siRNA transduction caused a significant reduction in *Abcb4*, but not *Abcg1,* mRNA expression (Fig. 6A). We found that the number, cell size and cell–cell fusion index of the OCLs formed in culture were attenuated by knockdown of *Abcg1* or *Abcb4* mRNAs in WT OCLs (Fig. 6B,C), whereas the mRNA expression of osteoclast differentiation-related molecules was not changed (Fig. S5).

Furthermore, we confirmed the role of ABCG1 in cell–cell fusion of OCLs using *Abcg1* sKO mice. As shown in Fig. 7A, the number of OCLs formed in the culture of *Abcg1* sKO OCL precursors in response to M-CSF and sRANKL decreased to 75% of that of WT OCLs. The average area and the fusion index were also reduced by approximately 50% of those in WT OCLs. Consistent with the decrease in OCL formation, PE translocation to the outer leaflet of the plasma membrane was also diminished by *Abcg1* gene deletion, indicating that ABCG1 abrogation caused impaired cell–cell fusion (Fig. 7B). The mRNA levels of osteoclast differentiation-related molecules in the *Abcg1* sKO osteoclastic cells were equivalent to the levels in WT cells during OCL formation (Fig. S6).

Liver X receptor is involved in OCL formation mediated by ABCG1 expression

Abcg1 is well known as a target gene of nuclear liver X receptor (LXR) (Sabol et al., 2005). Thus, we examined the effects of the LXR antagonist GSK 2033 (Griffett and Burris, 2016) and LXR agonist GW 3965 (Joseph et al., 2002) on OCL formation and on the mRNA levels of *Abcg1* in WT OCL culture in the presence of M-CSF and sRANKL. *LXRα* and *LXRβ* mRNAs were constantly expressed during OCL differentiation from WT OCL precursors (Fig. 8A). The addition of GSK 2033 to the culture of WT OCLs greatly attenuated OCL formation and decreased expression of *Abcg1* mRNA (Fig. 8B-D). In contrast, the addition of GW 3965 to the culture of LDLR sKO OCLs restored the expression of *Abcg1* mRNA up to approximately 140% of the expression level of WT OCLs. At the same time, the OCL formation also augmented and the increased number of OCLs became equivalent to the level of WT OCL formation (Fig. 8E-G). These results suggest the involvement of LXR in the cell–cell fusion of OCLs associated with PE translocation to the outer leaflet of the plasma membrane.

DISCUSSION

In this study, we demonstrated using *LDLR* sKO, *LDLR/LOX-1* dKO and *Abcg1* sKO mice that the uptake of LDL into OCL precursors via LDLR is pivotal for PE translocation from the inner to outer leaflet of the plasma membrane, in particular, of the filopodia; thereby, the multinucleation of OCLs through promoting cell–cell fusion proceeds. The *LDLR* sKO and *LDLR/LOX-1* dKO mice consistently exhibited reduced influx of LDL into the cells and the intracellular depletion of neutral lipids, including cholesterol, suggesting impaired intracellular *de novo* cholesterol biosynthesis. Consistent with the depleted status of intracellular cholesterol, the translocation of PE on the cell surface was impaired, and cell–cell fusion was subsequently reduced. The mRNA expression of ABCG1, a floppase that transfers phospholipids from the inner to outer leaflet of the plasma membrane, was greatly downregulated in response to sRANKL in the *LDLR* sKO and *LDLR/LOX-1* dKO OCL precursors, which coincided with reduced cell–cell fusion. In addition, *Abcg1* sKO mice showed reduced PE translocation on the cell surface and decreased cell–cell fusion of OCLs, similar to the *LDLR* sKO and *LDLR/LOX-1* dKO OCL precursors. Taken together, this study for the first time indicates that a novel cascade (LDLR∼ABCG1∼PE translocation to cell surface∼cell–cell fusion) plays an important role in OCL maturation, as described in Fig. S7.

So far, several studies have reported a close relationship between bone and lipid metabolisms. Both elevated levels of LDL and

Journal of Cell Science (2020) 133, jcs243840. doi:10.1242/jcs.243840

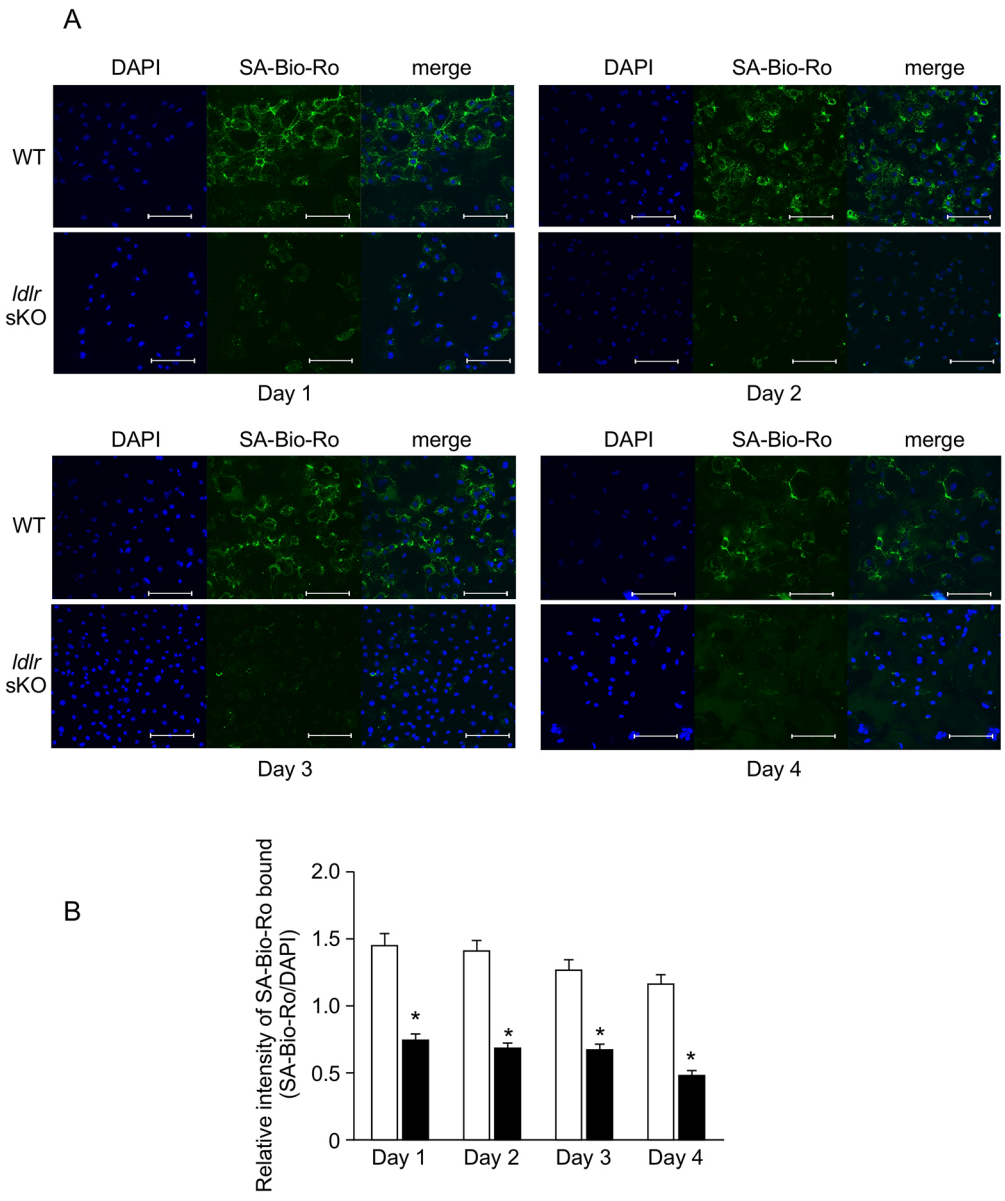

Fig. 5. Decreased level of PE in the outer leaflet of the plasma membrane of *LDLR* sKO OCLs. (A) WT and *LDLR* sKO OCL precursors were cultured with M-CSF and sRANKL for the indicated number of days. After the culture, OCLs were stained with SA–Bio-Ro (green) and DAPI (blue) and observed under a confocal laser microscope. (B) The relative intensity of SA–Bio-Ro per the intensity of DAPI in the culture of WT (open bars) and *LDLR* sKO (closed bars) OCLs was measured ($n \geq 25$). Experiments were performed in triplicate and reproducibility confirmed. Values represent the mean±s.e.m. *$P<0.05$ versus culture of WT OCLs. Scale bars: 100 µm.

decreased levels of high-density lipoprotein in plasma are correlated with low bone mass, and high triglyceride levels are associated with a decreased incidence of vertebral fractures in postmenopausal women (Yamaguchi et al., 2002). Patients with low bone densities and osteoporosis are characterized by elevated plasma lipid levels, more severe coronary atherosclerosis and an increased risk of stroke (Barengolts et al., 1998). Furthermore, an *in vivo* study demonstrated that a mouse strain with susceptibility to atherosclerosis (C57BL/6) lost a greater amount of bone mass in response to a high-fat diet than atherosclerosis-resistant strains (Parhami et al., 2001). Regarding osteoclastogenesis, we previously reported that deletion of LDLR causes reduced OCL formation as a result of impairment of cell–cell fusion of OCLs (Okayasu et al., 2012), whereby trabecular bone mass is increased due to the decrease in bone resorption. In contrast, the abrogation of LOX-1 promoted OCL formation following augmentation of cell–cell fusion, resulting in decreased bone volume (Nakayachi et al., 2015). Thus, the actions of LDLR and LOX-1 on osteoclastogenesis are opposing; that is, LDLR and LOX-1 are positive and negative regulators for bone resorption, respectively. However, the detailed molecular mechanism underlying the actions of LDLR and LOX-1 remained obscure. Initially, we presumed that the *LDLR/LOX-1* dKO mouse could be a control animal suitable for elucidating the mechanisms of both receptors and, therefore, we generated dKO mice. However, the phenotype of the *LDLR/LOX-1* dKO for OCL formation was similar to that of *LDLR* sKO, resulting in reduced osteoclast cell–cell fusion associated with decreased PE translocation on the cell surface. As a result, the impact of LDLR deletion exceeded that of LOX-1 abrogation regarding cell–cell fusion of OCLs.

Osteoclasts are a unique cell in the body and are responsible for bone resorption; mononuclear preosteoclasts are required for cell–cell fusion to acquire full osteoclast functions. Extensive studies have thus far revealed that several proteins, such as CD9, ATP6v0d2, DC-STAMP, OC-STAMP and dynamin, are involved in osteoclast cell–cell fusion during osteoclast differentiation in response to RANKL (Lee et al., 2006; Kim et al., 2010; Yagi et al., 2005; Ishii et al., 2006; Yang et al., 2008; Shin et al., 2014). In particular, *in vitro* overexpression of ATP6v0d2 and DC-STAMP augmented the formation of multinucleated OCLs (Kim et al., 2008). In addition, ATP6v0d2 and DC-STAMP knockout mice

Journal of Cell Science (2020) 133, jcs243840. doi:10.1242/jcs.243840

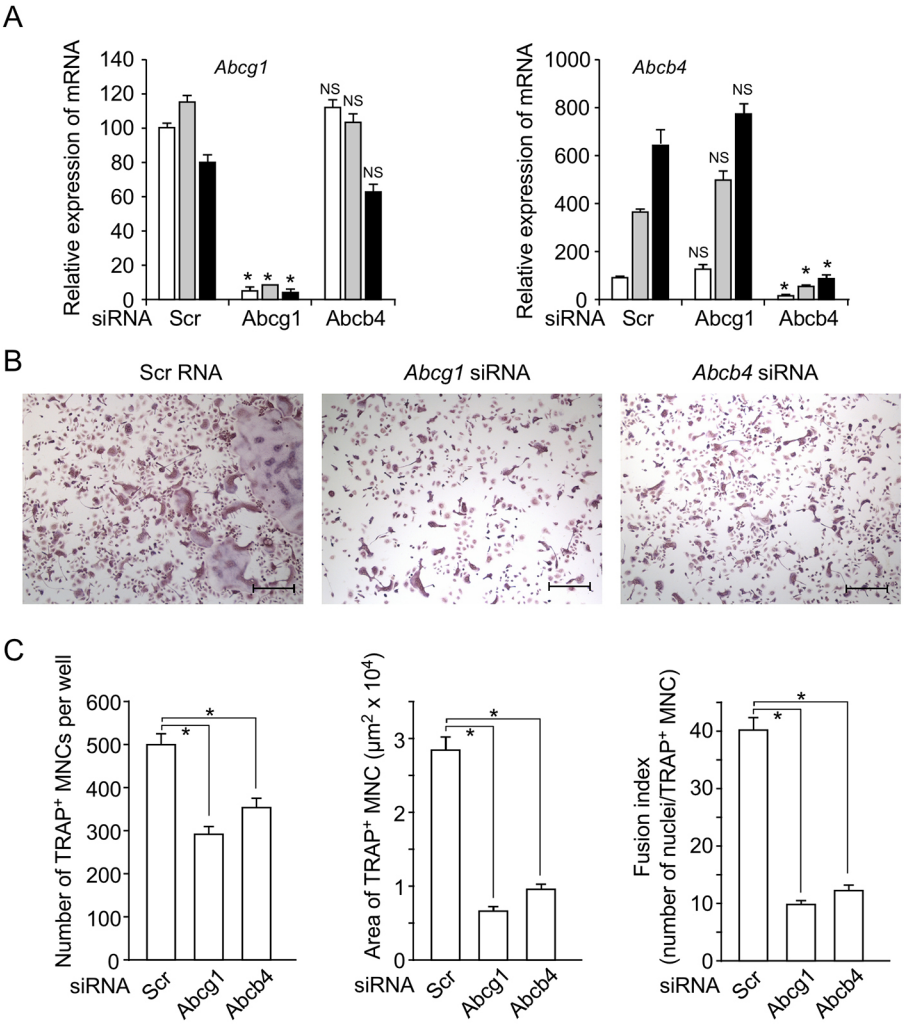

Fig. 6. Effect of knockdown of *Abcg1* mRNA and/or *Abcb4* mRNA on OCL formation. WT OCL precursors were electroporated with scramble RNA (Scr, 1 µM, negative control), *Abcg*1 siRNA (1 µM) or *Abcb4* siRNA (1 µM). (A) After transduction of the siRNAs, the OCL precursors were cultured with M-CSF and sRANKL. After culturing for 1 day (open bars), 2 days (gray bars) or 3 days (closed bars), the levels of *Abcg1* and *Abcb4* mRNAs were determined using quantitative real-time RT-PCR. Values represent the mean±s.d. (n=3). *P<0.05 versus culture of OCLs transduced by scramble RNA on each day. NS not significant. (B) Photographs of the culture with each siRNA on day 3. (C) After culturing for 3 days, the cells were stained for TRAP activity and the TRAP-positive MNCs counted (left). Experiments were performed in triplicate and reproducibility confirmed. Values represent the mean±s.d. (n=5). The average area and the fusion index of the TRAP-positive MNCs were also measured (middle and right). Values represent the mean±s.e.m. (n≥100). *P<0.05 versus culture of OCLs transduced by scramble RNA. Scale bars: 250 µm.

exhibited an increase in trabecular bone volume in parallel with a decrease in osteoclast formation (Lee et al., 2006; Yagi et al., 2005). However, the molecular mechanism of the actions of osteoclast fusion-related proteins has not yet been fully elucidated; for example, partner proteins, which interact with the fusion-related proteins, have not been identified. Cell–cell fusion is simply the fusion of the plasma membrane of a donor cell with the plasma membrane of a neighboring cell; that is, cell–cell fusion occurs through transfer of the plasma membrane phospholipid bilayer of two cells. Thus, cell–cell fusion cannot be interpreted only from the perspective of protein interactions but should also be considered from the viewpoint of the status change of the lipid bilayer of the plasma membrane. The interaction of phospholipids with osteoclast fusion-related proteins could also be important for understanding osteoclast cell–cell fusion.

The state of the plasma membrane lipid bilayer varies according to the species of phospholipids present in the outer and inner leaflets of the plasma membrane, depending on the size and hydrophilic properties of the head group of the phospholipids. When phosphatidylcholine with a relatively large polar head and sphingomyelin gather, the structure of the membrane becomes convex and tends to exist in the outer leaflet of the plasma membrane of spherical cells (Zimmerberg and Kozlov, 2006). On the other hand, PE, which has the smallest head and weak polarity, preferentially forms a concave structure. PE, along with PS, tends to be distributed in the inner leaflet of the plasma membrane (Zachowski, 1993). Thus, the phospholipid bilayers of the outer and inner leaflets exhibit asymmetric and different distributions of phospholipids, whereas the asymmetric structure is easily changed depending on cell function, motility and shape. Recently, Irie et al. (2017) demonstrated the relationship between changes in the PE distribution on the cell membrane and the cell–cell fusion of OCLs. The amount of PE in the cell surface increased with the differentiation of OCLs. In addition, gene knockdown of acyl-CoA:lysophosphatidylethanolamine acyltransferase 2 (catalyzing *de novo* PE biosynthesis), ABCB4 and ABCG1 reduced the amount of PE in the outer leaflet of the plasma membrane followed by a decrease in OCL formation, indicating the involvement of these enzymes in osteoclastogenesis. The results of this study also indicate that cell–cell fusion of OCLs and PE translocation to the outer leaflet of the cell membrane are associated with ABCG1. However, the expression profile of ABCG1 is controversial. Irie's group showed that the expression of mRNA and the cell surface PE level were increased during OCL differentiation in response to RANKL signaling (Irie et al. 2017). In contrast, our study indicated that ABCG1 expression was not elevated by RANKL addition, but rather, the RANKL stimulus reduced *Abcg1* mRNA expression to 50-70% of the level of untreated cells, suggesting that the RANKL signal is intrinsically suppressive for ABCG1 expression. However, the 50-70% reduction in *Abcg1* mRNA levels was maintained

Journal of Cell Science (2020) 133, jcs243840. doi:10.1242/jcs.243840

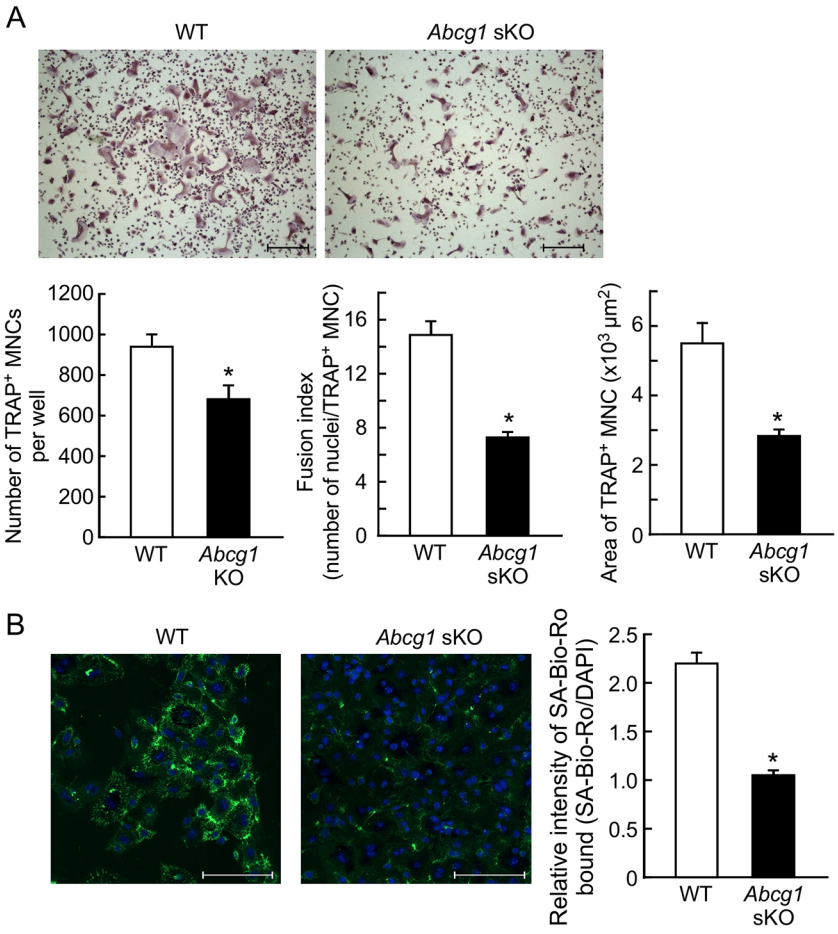

Fig. 7. Decreased *in vitro* OCL formation and phosphatidylethanolamine translocation to the outer leaflet of the plasma membrane in *Abcg1* KO OCLs. OCL precursors from WT and *Abcg1* KO bone marrow cells were cultured with sRANKL and M-CSF for 2 days. After culturing, the cells were stained for TRAP activity. (A) Top: Photographs of TRAP-positive OCLs that formed in the cultures. Bottom: The number of TRAP-positive MNCs with ≥3 nuclei (n=4). Values represent the mean±s.d. The fusion index and the average area of the TRAP-positive MNCs were also measured (n≥100 cells) in more than 100 TRAP-positive MNCs randomly selected in each culture. Values represent the mean±s.e.m. (B) The OCL precursors cultured with M-CSF and sRANKL for 2 days were incubated with SA–Bio-Ro and immunostained (green). The nuclei were also stained with DAPI (blue). Thereafter, the relative intensity of SA–Bio-Ro per the cell surface was measured (n≥100 cells). Values represent the mean± s.e.m. Experiments were performed in triplicate and reproducibility confirmed. *P<0.05 versus culture derived from WT mice. Scale bars: 250 µm (A), 100 µm (B).

without further reduction. Additionally, mononuclear OCL precursors and pre-OCLs already possessed a high level of PE in the outer leaflet of the plasma membrane, and the level was reduced at the stage of multinucleated OCLs. On the other hand, the expression of *Abcg*1 mRNA was markedly decreased in *LDLR* sKO and *LDLR/LOX-1* dKO OCLs compared with WT osteoclasts and, in parallel with the decrease, the PE distribution on the cell surface was also reduced. These results show that ABCG1 expression is decreased by RANKL stimulation, as described above, but that the decrease is ceased and maintained by the uptake of extracellular LDL via LDLR. Alternatively, a certain amount of ABCG1 could be maintained by increasing ABCG1 expression, dependent on extracellular LDL uptake.

Recently, Verma et al. (2018) reported that translocation of PS to the outer leaflet of the plasma membrane of OCLs is involved in cell–cell fusion. They treated mononuclear pre-OCLs with lysothosphatidylcholine to inhibit cell–cell fusion. After the removal of lysothosphatidylcholine, the authors evaluated the change in PS distribution on the cell surface and demonstrated that the interaction of cell surface PS with annexin A2 and annexin A5, which recognize PS on the cell surface, annexin-binding protein S100A4 and fusogenic protein syncyin 1 generates the driving force for cell–cell fusion. However, in this study, we could not detect PS translocation to the cell surface (data not shown), as reported by Irie et al. (2017). It is widely known that apoptotic cells externalize PS on the cell surface, producing an ‘eat me’ signal (Suzuki and Nagata, 2014). Annexin located on the cell surface of macrophages recognizes the cell surface PS; thereby, macrophages phagocytize apoptotic cells (Irie et al., 2017; Roelofs et al., 2010). Furthermore, PE is less hydrated than PS and fusion occurs easily when it comes into contact with the PE layer of an adjacent cell (Lis et al., 1982; Scheule, 1987). In contrast to PE, a highly hydrated PS layer repels the PS layer from each of the other cells. Therefore, PE could play a more important role than PS in efficient cell fusion. However, additional studies are needed to clarify the physiological involvement of both phospholipids in the OCL fusion process.

The translocation of phospholipids, sphingomyelin and cholesterol from the inner to outer leaflet of the plasma membrane is mediated by floppases, which include a variety of ABC transporters such as ABCAs, ABCBs, ABCCs and ABCGs (Coleman et al., 2013). In this study, we examined the expression of ABC transporters during OCL formation. Among the transporters, the expression of ABCB4 and ABCA2 was upregulated with OCL differentiation in response to RANKL signaling, whereas no difference in the expression profiles of the transporters was detected in the four OCL genotypes (WT, *LDLR/LOX-1* dKO, *LOX-1* sKO and *LDLR* sKO). Similarly, the expression patterns of ABCA1, ABCA3 and ABCG1 were not altered among the genotypes. Only the expression profile of ABCG1 was consistent with osteoclast formation; that is, although the expression levels in WT and LOX-1 OCLs were relatively maintained, the expression levels in *LDLR/LOX-1* dKO and *LDLR* sKO OCLs were markedly decreased, indicating correlation of ABCG1 with PE translocation and OCL formation. In addition, the expression of ABCG1 depends on LDL uptake. Although ABCG1 also mediates the efflux of cholesterol into high-density lipoprotein

Journal of Cell Science (2020) 133, jcs243840. doi:10.1242/jcs.243840

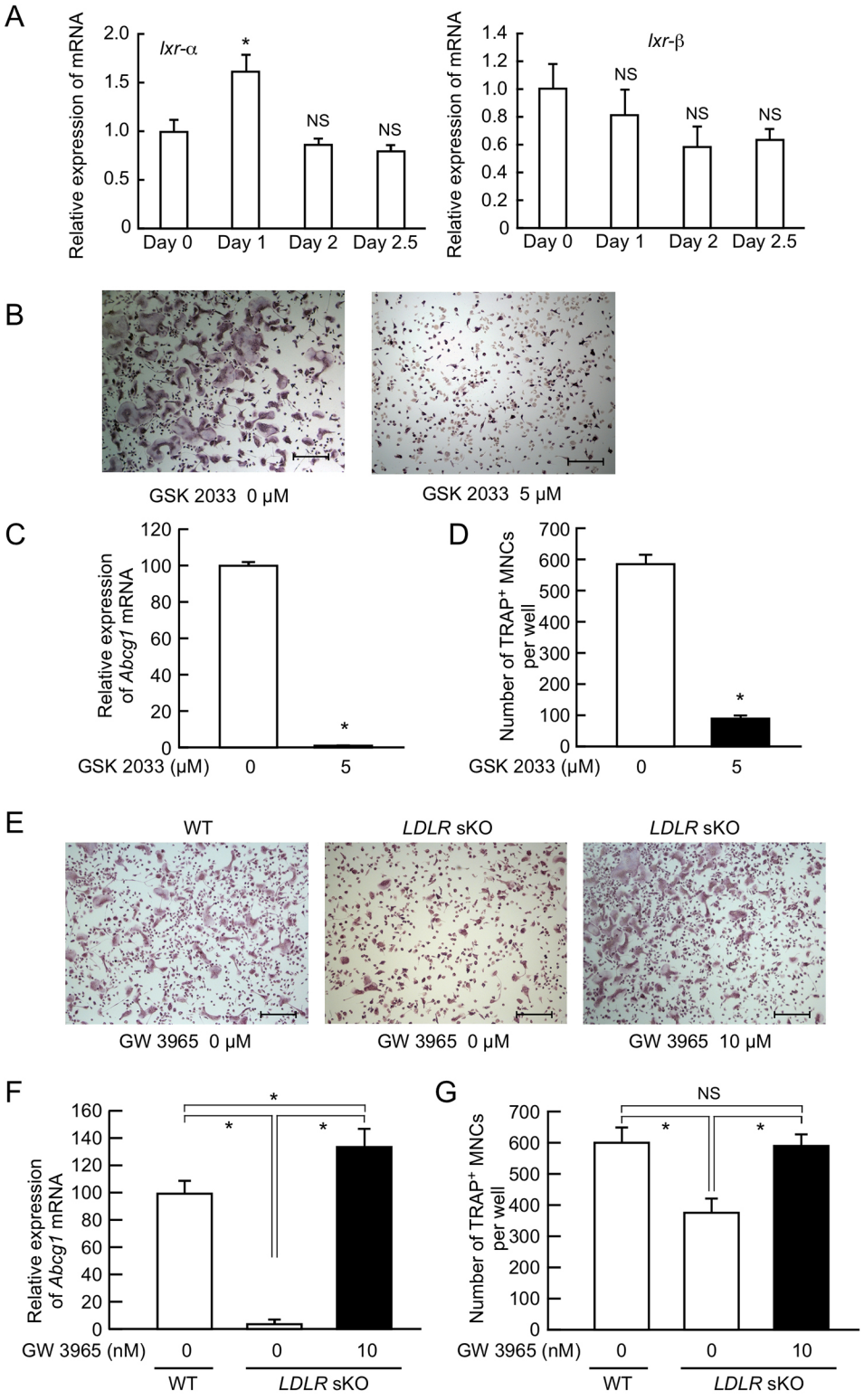

Fig. 8. Effect of GSK 2033, an antagonist of LXR, on osteoclastogenesis and expression of *Abcg1* mRNA in OCLs. (A) OCL precursors derived from WT mice were cultured with or without GSK 2033 (5 μM) in the presence of M-CSF and sRANKL for the indicated periods. After culturing, total RNA was prepared and the synthesized cDNA subjected to quantitative real-time RT-PCR to determine the levels of *lxr-α* and *lxr-β* mRNAs. Values represent the mean±s.d. (n=3). *P<0.05 and NS not significant versus culture on day 0. (B,D) WT bone marrow OCL precursors were treated with or without GSK 2033 (5 μM) for 2 days along with M-CSF and sRANKL. (B) Photographs of TRAP-positive OCLs that formed in the cultures. (D) OCLs were stained for TRAP activity to measure the number of TRAP-positive MNCs that formed in the culture. Values represent the mean±s.d. (n=4). *P<0.05 versus culture without GSK 2033. (E,G) WT and *LDLR* sKO OCL precursors were treated with or without GW 3965 (10 nM) for 2 days along with M-CSF and sRANKL. (E) Photographs of TRAP-positive OCLs that formed in the cultures. (G) OCLs were stained for TRAP activity to measure the number of TRAP-positive MNCs that formed in the culture. Values represent the mean±s.d. (n=4). *P<0.05 versus culture without GW 3965 or versus culture of WT OCLs without GW 3965. NS, not significant. (C,F) WT OCL precursors or *LDLR* sKO precursors were treated with GSK 2033 (C) or GW 3965 (F) for 1 day and the level of *Abcg1* mRNA measured using quantitative real-time RT-PCR. Values represent the mean±s.d. (n=3). *P<0.05 versus culture untreated with GSK 2033 (C); *P<0.05 versus culture without GW 3965, or *P<0.05 versus culture of WT OCLs without GW 3965 (G). Experiments were performed in triplicate (A-D) or in duplicate (E-G) and reproducibility confirmed. Scale bars: 250 μm.

and regulates lipid homeostasis (Schmitz et al., 2001), it remains controversial whether the transporter is involved in the transfer of PE to the cell surface. In this study, *Abcg1* sKO OCLs exhibited less translocation of PE to the outer leaflet of the plasma membrane and impaired cell–cell fusion. Thus, ABCG1 could mediate the efflux of various phospholipids as well as cholesterol. However, the distribution of PE and cholesterol on the osteoclastic cell surface differed; although cholesterol was ubiquitously distributed on the cell surface, the PE distribution was restricted to the filopodia. The results indicate that PE translocation depends on LDL uptake but that it differs from cholesterol translocation, suggesting cooperation of ABCG1 with another unknown translocation system.

RANKL/RANK signaling facilitates osteoclastogenesis via the activation of downstream signal transduction molecules such as c-Fos, NF-κB and NFATc1 (Asagiri and Takayanagi, 2007; Mizukami et al., 2002; Takayanagi et al., 2002). This study

Journal of Cell Science (2020) 133, jcs243840. doi:10.1242/jcs.243840

showed that RANKL/RANK signaling intrinsically represses ABCG1 expression. Indeed, it has been reported that the activation of NF-κB downregulates the expression of ABCG1 in RAW cells (Suzuki et al., 2017). Our results using *LDLR/LOX-1* dKO and *LDLR* sKO OCLs indicate that the downregulation becomes more pronounced by deletion of the *LDLR* gene; that is, the decrease in ABCG1 expression by the activation of NF-κB is reduced by LDL uptake through LDLR. The alleviation by LDL uptake may be attributed to the inhibition of downstream signaling pathways from the RANKL/RANK complex. Another mechanism for the reduction could be upregulation of ABCG1 expression by LDL incorporation into the cells. It has been reported that the expression of *Abcg1* is promoted by the nuclear transfer of the complex of LXR with retinoid X receptor or peroxisome proliferator-activated receptor-γ into the nucleus (Sabol et al., 2005; Uehara et al., 2007; Ozasa et al., 2011). The activation of LXR is provoked by intracellular oxysterol derived from cholesterol (Lehmann et al., 1997). As shown in this study, LXR blockage by the antagonist GSK 2033 reduced the expression of *Abcg1* mRNA followed by decreased osteoclast formation. On the other hand, LXR activation by the agonist GW 3965 restored the expression of *Abcg1* mRNA and the OCL formation. Together, these results suggest the involvement of LXR in osteoclast cell–cell fusion through the floppase activity of ABCG1.

In conclusion, PE translocation to the outer leaflet of the plasma membrane, which is mediated by ABCG1, is strictly dependent on LDL uptake via LDLR. PE translocation on the surface of filopodia is required for cell–cell fusion of OCLs. Our findings provide novel knowledge pertaining to the mechanism of cell–cell fusion of OCLs.

MATERIALS AND METHODS

Reagents

Recombinant human macrophage colony-stimulating factor (M-CSF) was kindly provided by Dr M. Yamada of the Morinaga Milk Industry Co. (Tokyo, Japan) and Prof. S. Suzu (Joint Research Center for Human Retrovirus Infection, Kumamoto University, Kumamoto, Japan). Recombinant murine soluble receptor activator of NF-κB ligand (sRANKL) was obtained from R&D Systems (Minneapolis, MN). LXR antagonist GSK 2033 and LXR agonist GW 3965 were purchased from Tocris Bioscience (Bristol, UK).

Mice

LOX-1$^{-/-}$ and *Abcg1*$^{-/-}$ mice have previously been described (Mehta et al., 2007; Draper et al., 2012). LDLR-deleted (*LDLR*$^{-/-}$) mice were obtained from The Jackson Laboratory (Bar Harbor, ME). The mice were maintained under specific pathogen-free conditions and were backcrossed into a C57BL/6J (CLEA Japan, Tokyo, Japan) background for a minimum of six generations. The experimental animal procedures were reviewed and approved by the Animal Care Committee of Meikai University School of Dentistry and conformed to relevant guidelines and laws. For the generation of *LDLR*$^{-/-}$*LOX-1*$^{-/-}$ dKO mice, male *LOX-1*$^{-/-}$ mice were first mated with female *LDLR*$^{-/-}$ mice to create *LDLR*$^{-/+}$*LOX-1*$^{-/+}$ mice. Then, the *LDLR*$^{-/+}$*LOX-1*$^{-/+}$ mice were mated with *LDLR*$^{-/-}$ mice to obtain *LDLR*$^{-/-}$*LOX-1*$^{-/+}$ mice. Finally, male *LDLR*$^{-/-}$*LOX-1*$^{-/+}$ mice were mated with female *LDLR*$^{-/-}$*LOX-1*$^{-/+}$ mice to generate *LDLR*$^{-/-}$*LOX-1*$^{-/-}$ mice. To determine the genotypes of WT and mutated *LOX-1* and *LDLR* genes, we used the primers described in Table S1. The resulting *LDLR*$^{-/-}$*LOX-1*$^{-/-}$ dKO mice were bred with each other and maintained under specific pathogen-free conditions on 12 h dark/12 h light cycles. The primer sequences used for the genotyping of *Abcg1*$^{-/-}$ and WT mice are indicated in Table S1.

In vitro assays for OCL formation from bone marrow monocytes treated with M-CSF and sRANKL

In vitro OCL formation has been previously described (Okayasu et al., 2012). Briefly, the femora and tibiae were obtained from 4- to 8-week-old male mice and the soft connective tissues removed from the bones. The bone marrow cells were flushed from the bone marrow cavity and cultured for 3 days in α-modified Eagle's minimum essential medium (α-MEM; Thermo Fisher Scientific, Rockford, IL) supplemented with 10% fetal bovine serum (FBS; Sigma-Aldrich, St Louis, MO), M-CSF (100 ng/ml) and 100 U/ml penicillin in Petri dishes in a humidified atmosphere of 5% CO_2. We used Petri dishes instead of tissue culture dishes to avoid the adhesion of bone marrow stromal cells on the dishes. Following the removal of the nonadherent cells and the small population of stromal cells by washing the dishes with PBS and subsequent incubation for 3 min in PBS containing 0.25% trypsin and 0.05% EDTA, the adherent monocytes were harvested for use as OCL precursors by vigorous pipetting in α-MEM containing 10% FBS. In the population of isolated OCL precursors, contaminating stromal cells represented less than 0.01% of the total cells, as described previously (Kaneda et al., 2000). The harvested OCL precursors were seeded in various tissue culture dishes and plates at an initial density of 2.5×10^4/cm^2 and cultured in α-MEM containing 10% FBS, M-CSF (20 ng/ml) and sRANKL (10 ng/ml). The culture medium was exchanged with fresh medium every 2 days. After culturing for the desired time, the cells were fixed in 10% formalin and stained for TRAP activity with a leukocyte acid phosphatase kit (Sigma-Aldrich). TRAP-positive multinucleated cells (MNCs) with more than three nuclei, which were considered OCLs, were counted under a microscope. The area of the multinucleated TRAP-positive MNCs was measured using the image analysis software Sensiv MEASURE (Mitani, Tokyo, Japan).

Assay of LDL uptake into OCL precursors treated with M-CSF and sRANKL

The uptake of LDL by osteoclast precursors was measured using the pHrod Red LDL uptake kit (Thermo Fisher Scientific) according to the manufacturer's instructions. Briefly, OCL precursors obtained from M-CSF-pretreated bone marrow cells were seeded at 1.6×10^5 cells/well and cultured with M-CSF (20 ng/ml) and sRANKL (10 ng/ml) in α-MEM containing 10% FBS for 6 h in each well of a polylysine-coated multiwell glass bottom culture dish (Matsunami, Osaka, Japan). After washing the cells once with PBS, the culture medium was replaced with LDL-starvation medium composed of FluoroBrite DMA (Thermo Fisher Scientific) plus 10% LDL-deficient serum (Biomedical Technologies, Stoughton, MA). The cells were cultured overnight with M-CSF and sRANKL to starve the cells of LDL. Thereafter, pHrode Red LDL (final concentration 10 µg/ml) was added to the culture and the cells incubated for 3 h at 37°C. For the negative control, cells were pretreated with unlabeled LDL (25 µg/ml) for 45 min prior to pHrode Red LDL labeling. For the last 30 min of labeling, the nuclei of the cells were stained with NucBlue live ReadyProbe reagent. Fluorescence images were obtained using a confocal laser microscope (LSM800, Carl Zeiss, Stuttgart, Germany).

Oil Red O staining of OCLs

OCL precursors were cultured in the presence of M-CSF and sRANKL in α-MEM containing 10% FBS for one day. Then, the cells were fixed with 3.7% formaldehyde in PBS for 15 min at room temperature, washed twice with PBS and then incubated in 60% 2-propanol for 1 min. Then, the cells were stained with Oil Red O solution (1.8 mg/ml of 60% 2-propanol) for 15 min. After staining, the cells were washed once with 60% 2-propanol and twice with PBS.

Staining of cell surface cholesterol of OCLs

To stain the cell surface cholesterol of OCLs, we employed θ-toxin-derived domain 4 (D4), which specifically binds cholesterol (Shimada et al., 2002). The pET28/His6-mCherry-D4 plasmid was obtained from Dr T. Kobayashi, RIKEN (Tsukuba, Japan). *Escherichia coli* strain BL21 (DE) was used for the overexpression of His-tag-mCherry D4 proteins. After induction by isopropyl β-D-1-thiogalactopyranoside, *E. coli* cells were harvested and lysed in HisTALON xTractor Buffer (Clontech Laboratories, Mountain View, CA) containing 10 units/ml DNase I and lysozyme solution. The overexpressed His-tag-mCherry-D4 proteins in the cell lysate were partially purified by TALON metal affinity resins in accordance with the manufacturer's instructions. Furthermore, the fractions eluted from the TALON metal affinity resins were applied to a butyl-agarose (Bio-Rad,

Hercules, CA) column equilibrated with 20 mM Tris-HCl (pH 7.5) containing 0.8 M $(NH_4)_2SO_4$. The cleaved His-tag-mCherry fragments did not bind to the hydrophobic resins. The bound His-tag-mCherry-D4 was eluted with 0.2 M $(NH_4)_2SO_4$, dialyzed against 20 mM Tris-HCl (pH 7.5) and concentrated using Amicon Ultra centrifugal filters (MWCO 10 kDa; Merck, Darmstadt, Germany). Finally, an equal volume of glycerol was added to the solution of His-tag-mCherry-D4. The protein concentration of the solution was measured and the solution stored at −20°C until use. The purity of His-tag-mCherry-D4 was confirmed to be more than 80% by SDS-PAGE analysis.

OCL precursors were cultured with M-CSF and sRANKL on polylysine-coated glass bottom culture dishes (Matsunami) for the indicated periods. Thereafter, the cells were treated with or without MβCD (10 mM) in BSA/HEPES/α-MEM [α-MEM containing 0.1% fatty acid-free BSA (Sigma-Aldrich) and 20 mM HEPES-NaOH, pH 7.4] for 30 min at 37°C. After washing once with BSA/HEPES/α-MEM, the cells were incubated in BSA/HEPES/α-MEM containing His-tag-mCherry-D4 (10 µg/ml) for 30 min. Then, the cells were quickly washed once with PBS and fixed with 4% paraformaldehyde in PBS for 15 min at room temperature. After washing with PBS, the nuclei of the cells were counterstained with 4′,6-diamidino-2-phenylindole (DAPI; Thermo Fisher Scientific). Fluorescence images were obtained using a confocal laser microscope (LSM800, Carl Zeiss).

Staining of phosphatidylethanolamine on the outer leaflet of the plasma membrane

To stain PE on the outer leaflet of the plasma membrane, we used Ro09-0198, which specifically recognizes and binds PE (Choung et al., 1988). Streptavidin (SA; Nacalai Tescue, Kyoto, Japan) was conjugated with biotinylated Ro09-0198 (Bio-Ro; provided by Dr M. Umeda, Kyoto University, Japan) and was dialyzed against PBS using Slide-A Lyzer (20,000 molecular weight cut off; Thermo Fisher Scientific) to separate free Bio-Ro in the solution.

OCL precursors were cultured with M-CSF and sRANKL on polylysine-coated glass bottom culture dishes (Matsunami) for the indicated periods. After washing once with BSA/HEPES/α-MEM prewarmed at 37°C, the cells were incubated with SA–Bio-Ro (5 µg/ml) in BSA/HEPES/α-MEM for 30 min at room temperature. Then, after washing once with BSA/HEPES/α-MEM, the cells were fixed with 3% paraformaldehyde in PBS for 30 min at room temperature and washed three times with PBS followed by 5 min of permeabilization with 0.1% TritonX-100 in PBS. Then, the cells were blocked with 3% BSA (Fraction V, Sigma-Aldrich) in PBS for 1 h prior to 1 h incubation with FITC-conjugated anti-SA-antibody (400-fold dilution; Vector Laboratories, Burlingame, CA) at room temperature. After incubation, the nuclei of cells were counterstained with a DAPI solution. We captured fluorescence images using a confocal laser microscope (LSM800, Carl Zeiss). The relative immunofluorescence intensity of SA–Bio-Ro on the cell surface was calculated as per the intensity of DAPI in the cells using ZEN2.1 (blue edition) software (Carl Zeiss).

Quantitative real-time PCR

The total RNA (100 ng) from cultured cells was used as the template for cDNA synthesis using a high-capacity RNA to cDNA kit (Thermo Fisher Scientific). Quantitative real-time PCR was performed using SsoAdvancedTM Universal Probes Supermix PCR (Bio-Rad) on a CFX Connect Real-Time PCR Detection System (Bio-Rad). TaqMan probes for the indicated genes were obtained from Thermo Fisher Scientific and are listed in Table S2. The relative expression of target mRNAs was quantified and normalized to the amount of 18S rRNA.

Statistical analysis

The data are presented as the mean±standard deviation (s.d.) or standard error of the mean (s.e.m.). The mean values of the groups were compared by unpaired Student's *t*-test or by one-way and two-way ANOVAs; the significance of the observed differences was subsequently determined by post hoc testing using Tukey's method and Bonferroni's method, respectively. $P<0.05$ was considered significant.

Acknowledgements

We thank Dr M. Yamada (Morinaga Milk Industry Co.) and Prof. S. Suzu (Joint Research Center for Human Retrovirus Infection, Kumamoto University) for providing the recombinant human M-CSF, and we thank Prof. M. Umeda (Kyoto University) for providing the biotin-conjugated Ro09-0198. We also appreciate Dr T. Kobayashi (RIKEN, and Directeur de recherche INSERM) for his help obtaining the pET28/His6-mCherry-D4 plasmid.

Competing interests

The authors declare no competing or financial interests.

Author contributions

Conceptualization: Y.H.; Methodology: V.J.F.K., Y.O., C.H., J.I., M.O., Y.H.; Validation: Y.H.; Formal analysis: J.I., Y.H.; Investigation: V.J.F.K., Y.O., C.H., J.I., M.O., T. Sato, T.O., M.T., Y.H.; Resources: V.J.F.K., Y.O., M.T., A.K., T. Sawamura, Y.H.; Writing - original draft: Y.H.; Writing - review & editing: V.J.F.K., Y.O., C.H., J.I., M.O., T. Sato, T.O., M.T., A.K., J.S., T. Sawamura; Visualization: Y.H.; Supervision: J.S., T. Sawamura, Y.H.; Project administration: J.S., Y.H.; Funding acquisition: Y.H.

Funding

This work was supported by the Japan Society for the Promotion of Science [Grant-in-Aid for Scientific Research (B), No. 16H05505 to Y.H.].

Supplementary information

Supplementary information available online at
http://jcs.biologists.org/lookup/doi/10.1242/jcs.243840.supplemental

Peer review history

The peer review history is available online at https://jcs.biologists.org/lookup/doi/10.1242/jcs.243840.reviewer-comments.pdf

References

Alagiakrishnan, K., Juby, A., Hanley, D., Tymchak, W. and Sclater, A. (2003). Role of vascular factors in osteoporosis. *J. Gerontol. A Biol. Sci. Med. Sci.* **58**, M362-M366. doi:10.1093/gerona/58.4.M362

Asagiri, M. and Takayanagi, H. (2007). The molecular understanding of osteoclast differentiation. *Bone* **40**, 251-264. doi:10.1016/j.bone.2006.09.023

Banks, L. M., Lees, B., MacSweeney, J. E. and Stevenson, J. C. (1994). Effect of degenerative spinal and aortic calcification on bone density measurements in post-menopausal women: links between osteoporosis and cardiovascular disease? *Eur. J. Clin. Invest.* **24**, 813-817. doi:10.1111/j.1365-2362.1994.tb02024.x

Barengolts, E. I., Berman, M., Kukreja, S. C., Kouznetsova, T., Lin, C. and Chomka, E. V. (1998). Osteoporosis and coronary atherosclerosis in asymptomatic postmenopausal women. *Calcif .Tissue Int.* **62**, 209-213. doi:10.1007/s002239900419

Chernomordik, L. V. and Kozlov, M. M. (2008). Mechanics of membrane fusion. *Nat. Struct. Mol. Biol.* **5**, 675-683. doi:10.1038/nsmb.1455

Choung, S.-Y., Kobayashi, T., Takemoto, K., Ishitsuka, H. and Inoue, K. (1988). Interaction of a cyclic peptide, Ro09-0198, with phosphatidylethanolamine in liposomal membranes. *Biochim. Biophys. Acta* **940**, 180-187. doi:10.1016/0005-2736(88)90193-9

Coleman, J. A., Quazi, F. and Molday, R. S. (2013). Mammalian P4-ATPases and ABC transporters and their role in phospholipid transport. *Biochim. Biophys. Acta* **1831**, 555-574. doi:10.1016/j.bbalip.2012.10.006

Draper, D. W., Gowdy, K. M., Madenspacher, J. H., Wilson, R. H., Whitehead, G. S., Nakano, H., Pandiri, A. R., Foley, J. F., Remaley, A. T., Cook, D. N. et al. (2012). ATP binding cassette transporter G1 deletion induces IL-17-dependent dysregulation of pulmonary adaptive immunity. *J. Immunol.* **188**, 5327-5336. doi:10.4049/jimmunol.1101605

Griffett, K. and Burris, T. P. (2016). Promiscuous activity of the LXR antagonist GSK2033 in a mouse model of fatty liver disease. *Biochem. Biophys. Res. Commun.* **479**, 424-428. doi:10.1016/j.bbrc.2016.09.036

Hada, N., Okayasu, M., Ito, J., Nakayachi, M., Hayashida, C., Kaneda, T., Uchida, N., Muramatsu, T., Koike, C., Masuhara, M. et al. (2012). Receptor activator of NF-κB ligand-dependent expression of caveolin-1 in osteoclast precursors, and high dependency of osteoclastogenesis on exogenous lipoprotein. *Bone* **50**, 226-236. doi:10.1016/j.bone.2011.10.028

Hankins, H. M., Baldridge, R. D., Xu, P. and Graham, T. R. (2015). Role of flippases, scramblases and transfer proteins in phosphatidylserine subcellular distribution. *Traffic* **16**, 35-47. doi:10.1111/tra.12233

Inaoka, T., Bilbe, G., Ishibashi, O., Tezuka, K., Kumegawa, M. and Kokubo, T. (1995). Molecular cloning of human cDNA for cathepsin K: novel cysteine proteinase predominantly expressed in bone. *Biochem. Biophys. Res. Commun.* **206**, 89-96. doi:10.1006/bbrc.1995.1013

Irie, A., Yamamoto, K., Miki, Y. and Murakami, M. (2017). Phosphatidylethanolamine dynamics are required for osteoclast fusion. *Sci. Rep.* **7**, 46715. doi:10.1038/srep46715
Ishii, M., Iwai, K., Koike, M., Ohshima, S., Kudo-Tanaka, E., Ishii, T., Mima, T., Katada, Y., Miyatake, K., Uchiyama, Y. et al. (2006). RANKL-induced expression of tetraspanin CD9 in lipid raft membrane microdomain is essential for cell fusion during osteoclastogenesis. *J. Bone Miner. Res.* **21**, 965-976. doi:10.1359/jbmr.060308
Joseph, S. B., McKilligin, E., Pei, L., Watson, M. A., Collins, A. R., Laffitte, B. A., Chen, M., Noh, G., Goodman, J., Hagger, G. N. et al. (2002). Synthetic LXR ligand inhibits the development of atherosclerosis in mice. *Proc. Natl. Acad. Sci. USA* **99**, 7604-7609. doi:10.1073/pnas.112059299
Kaneda, T., Nojima, T., Nakagawa, M., Ogasawara, A., Kaneko, H., Sato, T., Mano, H., Kumegawa, M. and Hakeda, Y. (2000). Endogenous production of TGF-β is essential for osteoclastogenesis induced by a combination of receptor activator of NF-κB ligand and macrophage-colony-stimulating factor. *J. Immunol.* **165**, 4254-4263. doi:10.4049/jimmunol.165.8.4254
Kim, K., Lee, S.-H., Ha Kim, J., Choi, Y. and Kim, N. (2008). NFATc1 induces osteoclast fusion via up-regulation of Atp6v0d2 and the dendritic cell-specific transmembrane protein (DC-STAMP). *Mol. Endocrinol.* **22**, 176-185. doi:10.1210/me.2007-0237
Kim, T., Ha, H., Kim, N., Park, E.-S., Rho, J., Kim, E. C., Lorenzo, J., Choi, Y. and Lee, S. H. (2010). ATP6v0d2 deficiency increases bone mass, but does not influence ovariectomy-induced bone loss. *Biochem. Biophys. Res. Commun.* **403**, 73-78. doi:10.1016/j.bbrc.2010.10.117
Lee, S.-H., Rho, J., Jeong, D., Sul, J.-Y., Kim, T., Kim, N., Kang, J.-S., Miyamoto, T., Suda, T., Lee, S.-K. et al. (2006). v-ATPase V0 subunit d2-deficient mice exhibit impaired osteoclast fusion and increased bone formation. *Nat. Med.* **12**, 1403-1409. doi:10.1038/nm1514
Lehmann, J. M., Kliewer, S. A., Moore, L. B., Smith-Oliver, T. A., Oliver, B. B., Su, J.-L., Sundseth, S. S., Winegar, D. A., Blanchard, D. E., Spencer, T. A. et al. (1997). Activation of the nuclear receptor LXR by oxysterols defines a new hormone response pathway. *J. Biol. Chem.* **272**, 3137-3140. doi:10.1074/jbc.272.6.3137
Lis, L. J., McAlister, M., Fuller, N., Rand, R. P. and Parsegian, V. A. (1982). Interactions between neutral phospholipid bilayer membranes. *Biophys. J.* **37**, 657-665.
Mehta, J. L., Sanada, N., Hu, C. P., Chen, J., Dandapat, A., Sugawara, F., Satoh, H., Inoue, K., Kawase, Y., Jishage, K. et al. (2007). Deletion of LOX-1 reduces atherogenesis in LDLR knockout mice fed high cholesterol diet. *Circ. Res.* **100**, 1634-1642. doi:10.1161/CIRCRESAHA.107.149724
Mensah, K. A., Ritchlin, C. T. and Schwarz, E. M. (2010). RANKL induces heterogeneous DC-STAMP(lo) and DC-STAMP(hi) osteoclast precursors of which the DC-STAMP(lo) precursors are the master fusogens. *J. Cell. Physiol.* **223**, 76-83. doi:10.1002/jcp.22012
Mizukami, J., Takaesu, G., Akatsuka, H., Sakurai, H., Ninomiya-Tsuji, J., Matsumoto, K. and Sakurai, N. (2002). Receptor activator of NF-kappaB ligand (RANKL) activates TAK1 mitogen-activated protein kinase kinase kinase through a signaling complex containing RANK, TAB2, and TRAF6. *Mol. Cell. Biol.* **22**, 992-1000. doi:10.1128/MCB.22.4.992-1000.2002
Montigny, C., Lyons, J., Champeil, P., Nissen, P. and Lenoir, G. (2016). On the molecular mechanism of flippase- and scramblase-mediated phospholipid transport. *Biochim. Biophys. Acta* **1861**, 767-783. doi:10.1016/j.bbalip.2015.12.020
Nakayachi, M., Ito, J., Hayashida, C., Ohyama, Y., Kakino, A., Okayasu, M., Sato, T., Ogasawara, T., Kaneda, T., Suda, N. et al. (2015). Lectin-like oxidized low-density lipoprotein receptor-1 abrogation causes resistance to inflammatory bone destruction in mice, despite promoting osteoclastogenesis in the steady state. *Bone* **75**, 170-182. doi:10.1016/j.bone.2015.02.025
Okayasu, M., Nakayachi, M., Hayashida, C., Ito, J., Kaneda, T., Masuhara, M., Suda, N., Sato, T. and Hakeda, Y. (2012). Low-density lipoprotein receptor deficiency causes impaired osteoclastogenesis and increased bone mass in mice because of defect in osteoclastic cell-cell fusion. *J. Biol. Chem.* **287**, 19229-19241. doi:10.1074/jbc.M111.323600
Oren-Suissa, M. and Podbilewicz, B. (2007). Cell fusion during development. *Trends Cell Biol.* **17**, 537-546. doi:10.1016/j.tcb.2007.09.004
Ozasa, H., Ayaori, M., Iizuka, M., Terao, Y., Uto-Kondo, H., Yakushiji, E., Takiguchi, S., Nakaya, K., Hisada, T., Uehara, Y. et al. (2011). Pioglitazone enhances cholesterol efflux from macrophages by increasing ABCA1/ABCG1expressions via PPARγ/LXRα pathway: findings from in vitro and ex vivo studies. *Atherosclerosis* **219**, 141-150. doi:10.1016/j.atherosclerosis.2011.07.113
Parhami, F., Tintut, Y., Beamer, W. G., Gharavi, N., Goodman, W. and Demer, L. L. (2001). Atherogenic high-fat diet reduces bone mineralization in mice. *J. Bone Miner. Res.* **16**, 182-188. doi:10.1359/jbmr.2001.16.1.182
Pinals, R. S. and Jabbs, J. M. (1972). Type-IV hyperlipoproteinaemia and transient osteoporosis. *Lancet* **2**, 929. doi:10.1016/S0140-6736(72)92571-8
Roelofs, A. J., Thompson, K., Ebetino, F. H., Rogers, M. J. and Coxon, F. P. (2010). Bisphosphonates: molecular mechanisms of action and effects on bone cells, monocytes and macrophages. *Curr. Pharm. Des.* **16**, 2950-2960. doi:10.2174/138161210793563635
Sabol, S. L., Brewer, H. B., Jr and Santamarina-Fojo, S. (2005). The human ABCG1 gene: identification of LXR response elements that modulate expression in macrophages and liver. *J. Lipid Res.* **46**, 2151-2167. doi:10.1194/jlr.M500080-JLR200
Scheule, R. K. (1987). Fusion of Sindbis virus with model membranes containing phosphatidylethanolamine: implications for protein-induced membrane fusion. *Biochim. Biophys. Acta* **899**, 185-195. doi:10.1016/0005-2736(87)90399-3
Schmitz, G., Langmann, T. and Heimerl, S. (2001). Role of ABCG1 and other ABCG family members in lipid metabolism. *J. Lipid Res.* **42**, 1513-1520.
Shimada, Y., Maruya, M., Iwashita, S. and Ohno-Iwashita, Y. (2002). The C-terminal domain of perfringolysin O is an essential cholesterol-binding unit targeting to cholesterol-rich microdomains. *Eur. J. Biochem.* **269**, 6195-6203. doi:10.1046/j.1432-1033.2002.03338.x
Shin, N.-Y., Choi, H., Neff, L., Wu, Y., Saito, H., Ferguson, S. M., De Camilli, P. and Baron, R. (2014). Dynamin and endocytosis are required for the fusion of osteoclasts and myoblasts. *J. Cell Biol.* **207**, 73-89. doi:10.1083/jcb.201401137
Suzuki, J. and Nagata, S. (2014). Phospholipid scrambling on the plasma membrane. *Methods Enzymol.* **544**, 381-393. doi:10.1016/B978-0-12-417158-9.00015-7
Suzuki, J., Umeda, M., Sims, P. J. and Nagata, S. (2010). Calcium-dependent phospholipid scrambling by TMEM16F. *Nature* **468**, 834-838. doi:10.1038/nature09583
Suzuki, K., Kawakami, Y. and Yamauchi, K. (2017). Impact of TLR 2, TLR 4-activation on the expression of ABCA1 and ABCG1 in raw cells. *Ann. Clin. Lab. Sci.* **47**, 436-446.
Takayanagi, H., Kim, S., Koga, T., Nishina, H., Isshiki, M., Yoshida, H., Saiura, A., Isobe, M., Yokochi, T., Inoue, J. et al. (2002). Induction and activation of the transcription factor NFATc1 (NFAT2) integrate RANKL signaling in terminal differentiation of osteoclasts. *Dev. Cell* **3**, 889-901. doi:10.1016/S1534-5807(02)00369-6
Teitelbaum, S. L. (2007). Osteoclasts: what do they do and how do they do it? *Am. J. Pathol.* **170**, 427-435. doi:10.2353/ajpath.2007.060834
Uehara, Y., Miura, S., von Eckardstein, A., Abe, S., Fujii, A., Matsuo, Y., Rust, S., Lorkowski, S., Assmann, G., Yamada, T. et al. (2007). Unsaturated fatty acids suppress the expression of the ATP-binding cassette transporter G1 (ABCG1) and ABCA1 genes via an LXR/RXR responsive element. *Atherosclerosis* **191**, 11-21. doi:10.1016/j.atherosclerosis.2006.04.018
van Meer, G., Voelker, D. R. and Feigenson, G. W. (2008). Membrane lipids: where they are and how they behave. *Nat. Rev. Mol. Cell Biol.* **9**, 112-124. doi:10.1038/nrm2330
Verma, S. K., Leikina, E., Melikov, K., Gebert, C., Kram, V., Young, M. F., Uygur, B. and Chernomordik, L. V. (2018). Cell-surface phosphatidylserine regulates osteoclast precursor fusion. *J. Biol. Chem.* **293**, 254-270. doi:10.1074/jbc.M117.809681
Xing, L., Xiu, Y. and Boyce, B. F. (2012). Osteoclast fusion and regulation by RANKL-dependent and independent factors. *World J. Orthop.* **3**, 212-222. doi:10.5312/wjo.v3.i12.212
Yagi, M., Miyamoto, T., Sawatani, Y., Iwamoto, K., Hosogane, N., Fujita, N., Morita, K., Ninomiya, K., Suzuki, T., Miyamoto, K. et al. (2005). DC-STAMP is essential for cell-cell fusion in osteoclasts and foreign body giant cells. *J. Exp. Med.* **202**, 345-351. doi:10.1084/jem.20050645
Yamaguchi, T., Sugimoto, T., Yano, S., Yamauchi, M., Sowa, H., Chen, Q. and Chihara, K. (2002). Plasma lipids and osteoporosis in postmenopausal women. *Endocr. J.* **49**, 211-217. doi:10.1507/endocrj.49.211
Yang, M., Birnbaum, M. J., MacKay, C. A., Mason-Savas, A., Thompson, B. and Odgren, P. R. (2008). Osteoclast stimulatory transmembrane protein (OC-STAMP), a novel protein induced by RANKL that promotes osteoclast differentiation. *J. Cell. Physiol.* **215**, 497-505. doi:10.1002/jcp.21331
Yasuda, H., Shima, N., Nakagawa, N., Yamaguchi, K., Kinosaki, M., Mochizuki, S., Tomoyasu, A., Yano, K., Goto, M., Murakami, A. et al. (1998). Osteoclast differentiation factor is a ligand for osteoprotegerin/osteoclastogenesis-inhibitory factor and is identical to TRANCE/RANKL. *Proc. Natl. Acad. Sci. USA* **95**, 3597-3602. doi:10.1073/pnas.95.7.3597
Yoshimoto, R., Fujita, Y., Kakino, A., Iwamoto, S., Takaya, T. and Sawamura, T. (2011). The discovery of LOX-1, its ligands and clinical significance. *Cardiovasc. Drugs Ther.* **25**, 379-391. doi:10.1007/s10557-011-6324-6
Zachowski, A. (1993). Phospholipids in animal eukaryotic membranes: transverse asymmetry and movement. *Biochem. J.* **294**, 1-14. doi:10.1042/bj2940001
Zhou, X. and Graham, T. R. (2009). Reconstitution of phospholipid translocase activity with purified Drs2p, a type-IV P-type ATPase from budding yeast. *Proc. Natl. Acad. Sci. USA* **106**, 16586-16591. doi:10.1073/pnas.0904293106
Zimmerberg, J. and Kozlov, M. M. (2006). How proteins produce cellular membrane curvature. *Nat. Rev. Mol. Cell Biol.* **7**, 9-19. doi:10.1038/nrm1784

Supplementary information

Table S1. Primer sequence used for gentyping of LDLR and LOX-1 KO mice.

LDLR primers:

oIMR$_{5284}$, 5'- GTCTGCGAATAGGCTGGTGTAAGCCATAGC-3'; (Primer-3, P-3)

oIMR$_{5285}$, 5'- GATTGGGAAGACAATAGCAGGCATGC -3'; (Primer-E, P-E)

oIMR$_{5286}$, 5'- TTTGAACTCAGGACTTCGTGCTCTGGCAGC -3'; (Primer-4, P-4)

LOX-1 primers:

LOX-1-1485F-2, 5'-CCTCGTGCTTTACGGTATCGCC-3'

LOX-1(genetype)Del1064-F,5'-CCTTCAAGACGGAGCTGTGTTCGCTG-3'

LOX-1(genotype)-R, 5'-CCAGGTCAGGCAGGAAGCATCATTTA-3'

ABCG1 primers:

G1 E, 5'-GGGATCTCTGGGAAATTCAACAGTG-3'

G1ET, 5'-GTGAGCAGAGCTTCTGGTAGCAAAC-3'

Neo, 5'-GGGCCAGCTCATTCCTCCCACTCAT-3'

Table S2. Taqman probe ID.

c-Fos mRNA (*c-Fos*, Mm00487425_m1)
NFATc1 mRNA (*Nfatc1,* Mm00479445_m1)
TRAP mRNA (*Acp5,* Mm00475698_m1)
cathepsin K mRNA (*Ctsk* , Mm00484039_m1)
DC-STAMP mRNA (*Dcstamp*, Mm04209236_m1)
OC-STAMP mRNA (*Ocstamp*, Mm00512445_m1)
ATA6v0d2 mRNA (*Atp6v0d2,* Mm01222963_m1)
ABCA1 mRNA (*Abca1,* Mm00442646_m1)
ABCA2 mRNA (*Abca2,* Mm00431553_m1)
ABCA3 mRNA (*Abca3,* Mm00550501_m1)
ABCA4 mRNA (*Abca4,* Mm00492035_m1)
ABCB1 mRNA (*Abcb1α,* Mm00440761_m1)
ABCB1 mRNA (*Abcb1β,* Mm00440736_m1)
ABCB4 mRNA (*Abcb4,* Mm00435630_m1)
ABCG1 mRNA (*Abcg1,* Mm00437390_m1)
ABCG4 mRNA (*Abcg4,* Mm00507247_m1)
LXRα mRNA (*Lxr-α*, Mm00443451_ml)
LXRβ mRNA (*Lxr-β*, Mm00437265_ml)
18S rRNA (Mm03928990_g1)

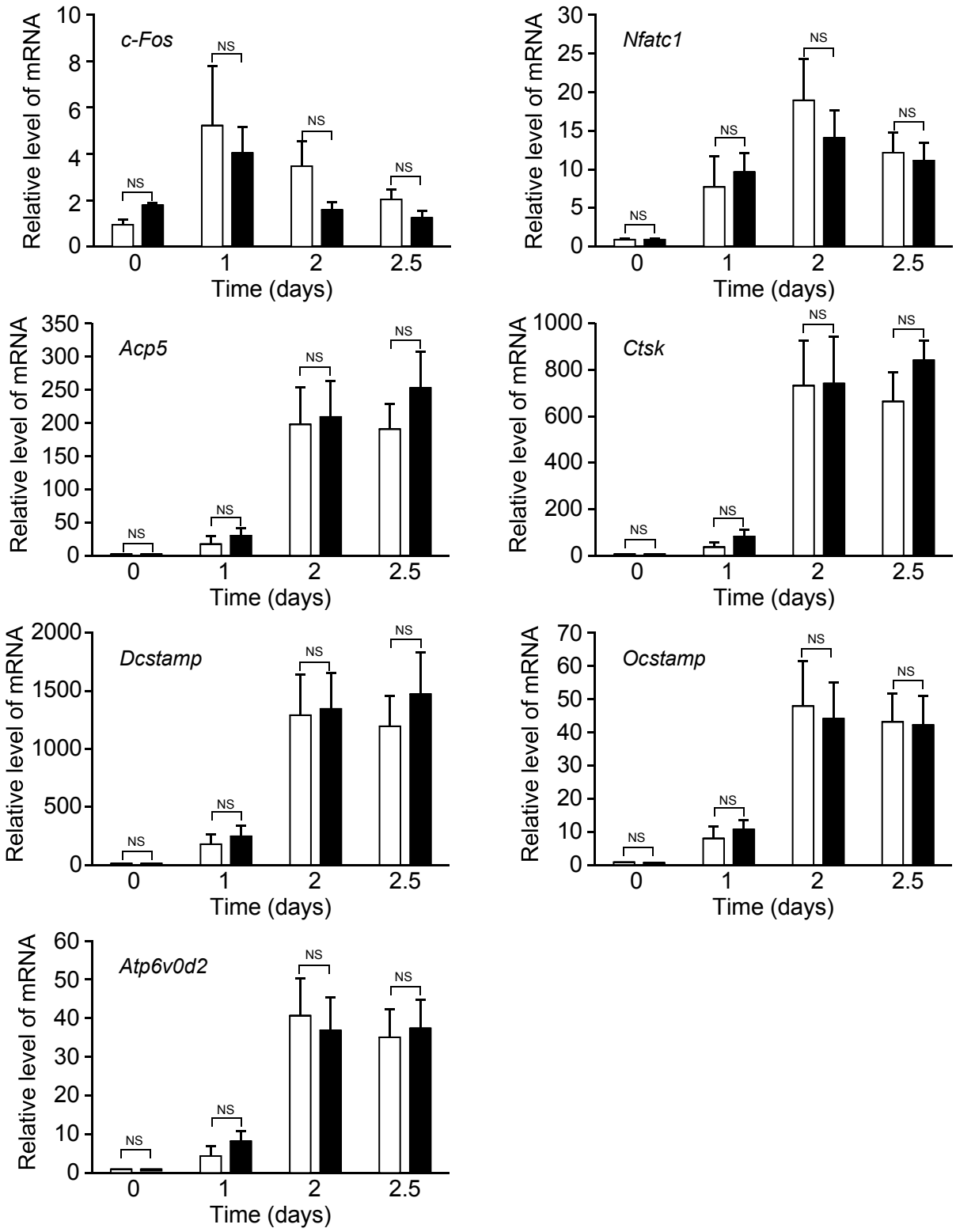

Fig. S1. Expression of osteoclast differentiation-related genes in *LDLR1/LOX-1* double knockout (dKO) OCLs. OCL-precursors from wild-type (WT, open bars) and *LDLR1/LOX-1* dKO (closed bars) bone marrow cells were cultured with sRANKL (10 ng/ml) and M-CSF (20 ng/ml) for the indicated days. After culture, total RNA was prepared, and the synthesized cDNA was subjected to quantitative real-time RT-PCR to determine the mRNA levels of c-Fos (*c-Fos*), NFATc1 (*Nfatc1*), TRAP (*Acp5*), cathepsin K (*Ctsk*), DC-STAMP (*Dcstamp*), OC-STAMP (*Ocstamp*) and ATP6v0d2 (*Atp6v0d2*) during osteoclastogenesis. The values represent the mean ± SD (n = 3). *NS* means that the difference was not significant between the cultures of WT and dKO OCLs on each day.

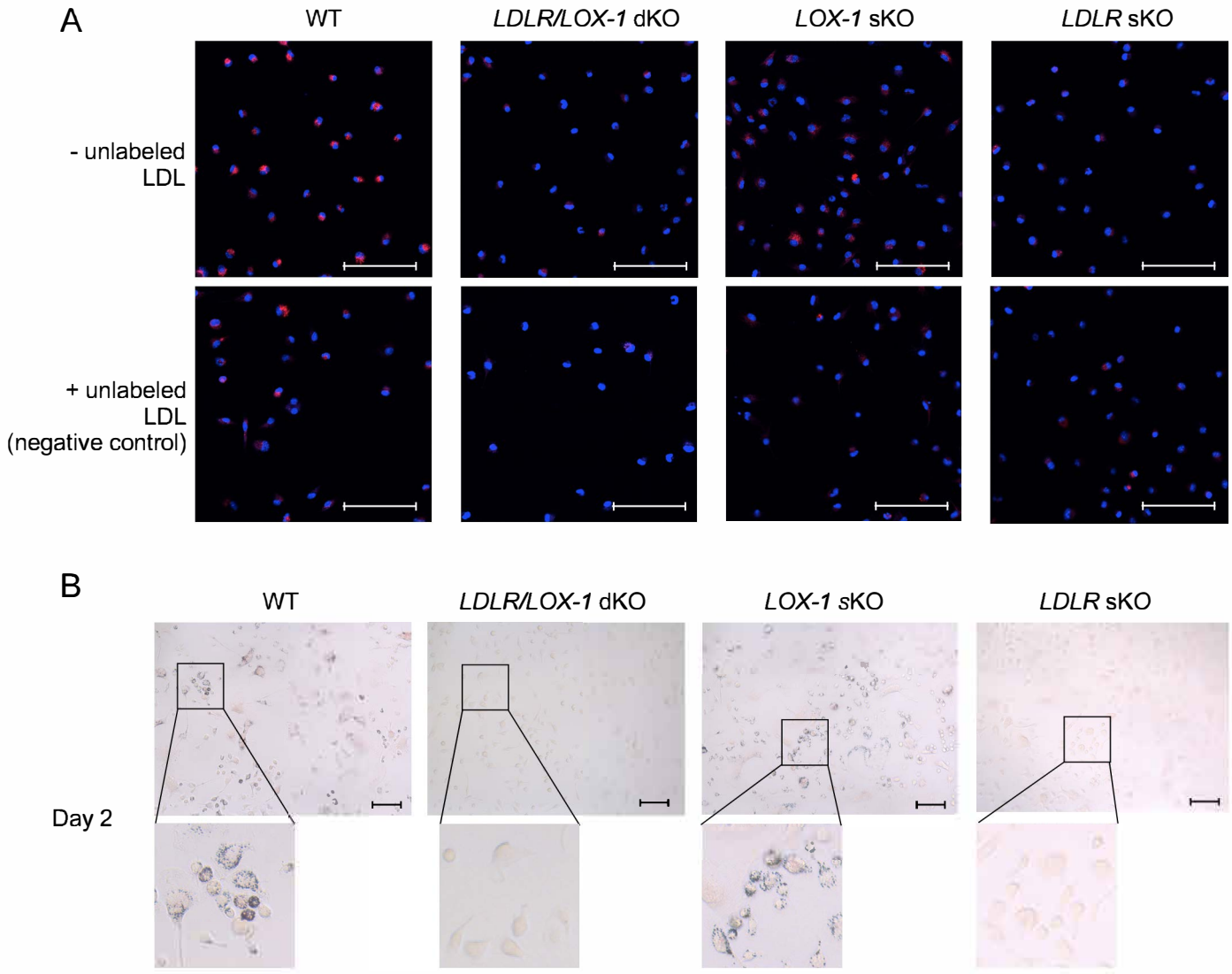

Fig. S2. Uptake of LDL into osteoclastic cells f om WTand *LDLR1 LOX-1* d O OCL-precursors and the accumulation of neut al lipids, including choleste ol, in the cells. (A) After OCL-precursors of WT, *LDLR/LOX-1* double KO (dKO), *LOX-1* single KO (sKO) and *LDLR* sKO mice were starved for exogenous LDL overnight, the cells were incubated with pHrodo^{TM} Red-labeled LDL for 3 h prior to counterstaining the nuclei. For the negative control, cells were pretreated with unlabeled LDL for 1 h. Scale bars, 100 µm. (B) For Oil Red O staining for intracellular neutral lipids, including cholesterol, the OCL-precursors were treated with M-CSF and sRANKL for 2 days and stained with Oil Red O solution. The scale bars (upper panels in (B)) indicate 100 µm, and the square areas were expanded (lower panels). The experiments were performed in triplicate, and reproducibility was confirmed.

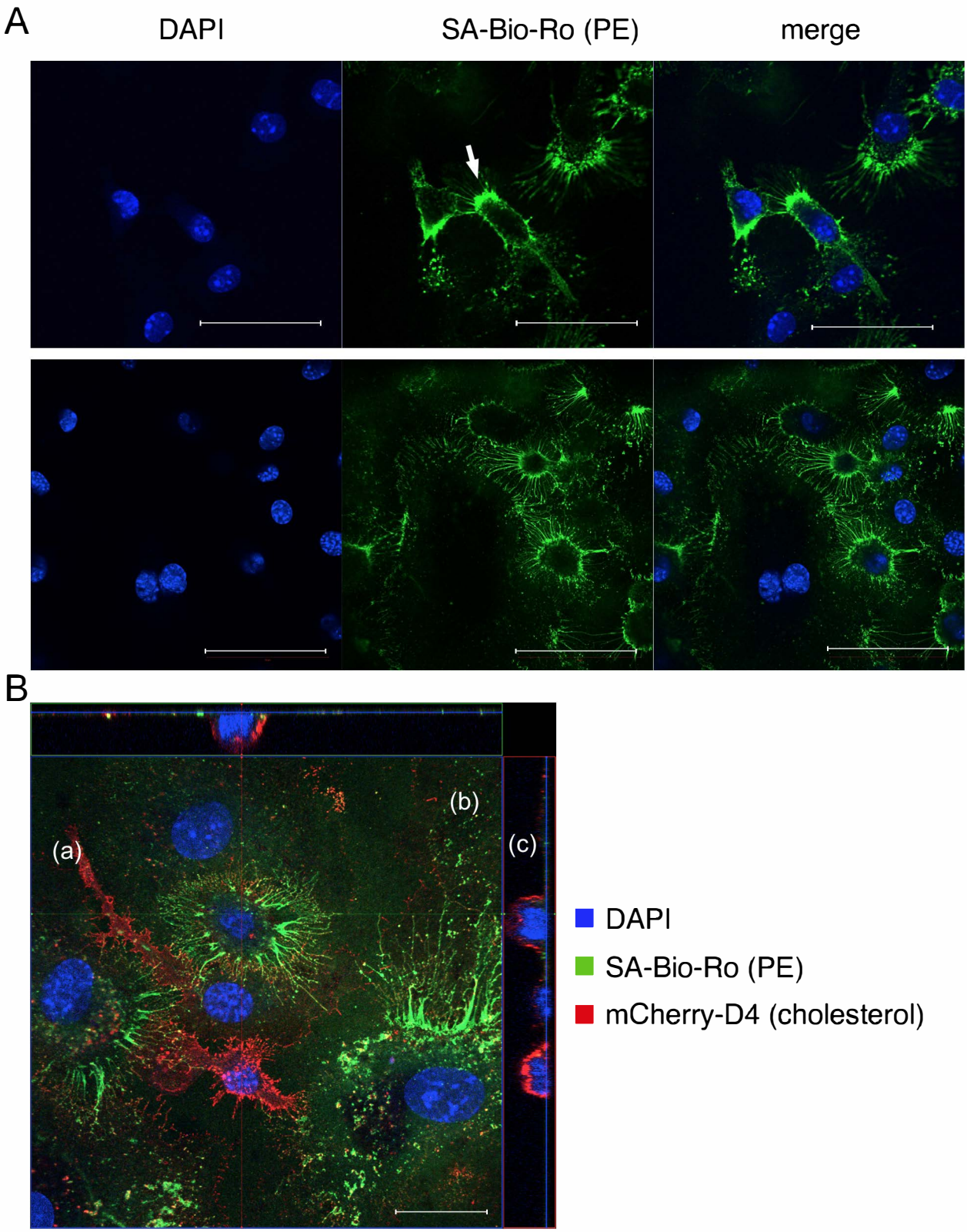

Fig. S3. Distributions of PE and cholesterol on the cell surface of osteoclastic cells. WT OCLs cultured with M-CSF and sRANKL for 2 days were incubated with SA-Bio-Ro for 30 min, and thereafter, the cells were fixed and immunostained by FITC-conjugated anti-SA antibody. The nuclei of the OCLs were counterstained with DAPI. The cells were observed by confocal laser microscopy. Scale bar, 20 µm. (B) The OCLs were simultaneously incubated with both SA-Bio-Ro and His-tag-mCherry-D4. After fixation, the cells were immunostained with anti-SA antibody. Thirty-five-slice images from the bottom to the top of the cells were obtained using a Z-stack method of confocal laser microscopy, and then, the images were reconstructed. (a), XY-image. (b) and (c), XZ-images. Scale bar, 10 µm.

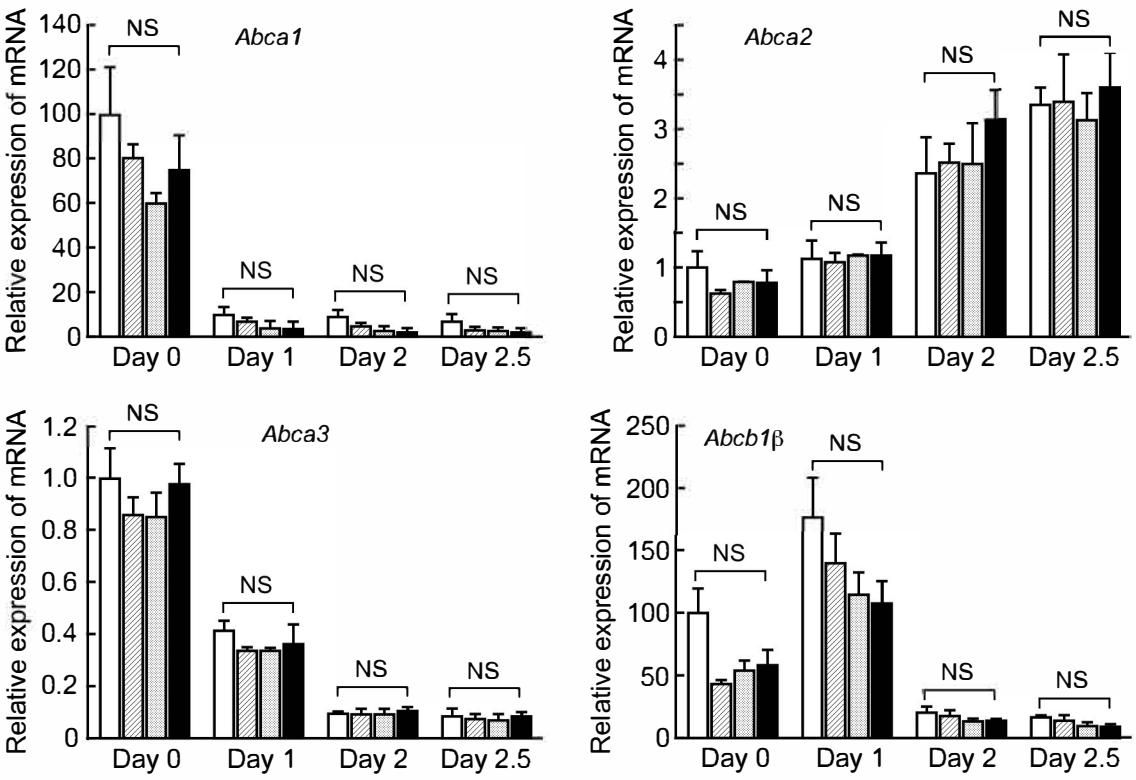

Fig. S4. mRNA expression of ABC transporters, in addition to ABCB4 and ABCG1, in OCLs with four different genotypes. Osteoclast precursors from WT (open bars), *LOX-1* single KO (sKO, hatched bars), *LDLR* sKO (dotted bars) and *LDLR1/LOX-1* dKO (closed bars) bone marrow cells were cultured with sRANKL (10 ng/ml) and M-CSF (20 ng/ml) for the indicated days. After culture, total RNA was prepared, and the synthesized cDNA was subjected to quantitative real-time RT-PCR to determine the mRNA levels of ABCA1 (*Abca1*), ABCA2 (*Abca2*), ABCA3 (*Abca3*) and ABCB1 (*Abcb1*) during osteoclastogenesis. The experiments were performed in triplicate, and reproducibility was confirmed. The values represent the mean ± SD (n = 3). *NS* means that the difference was not significant between the cultures of WT cells and each KO OCLs of each other genotype on each day.

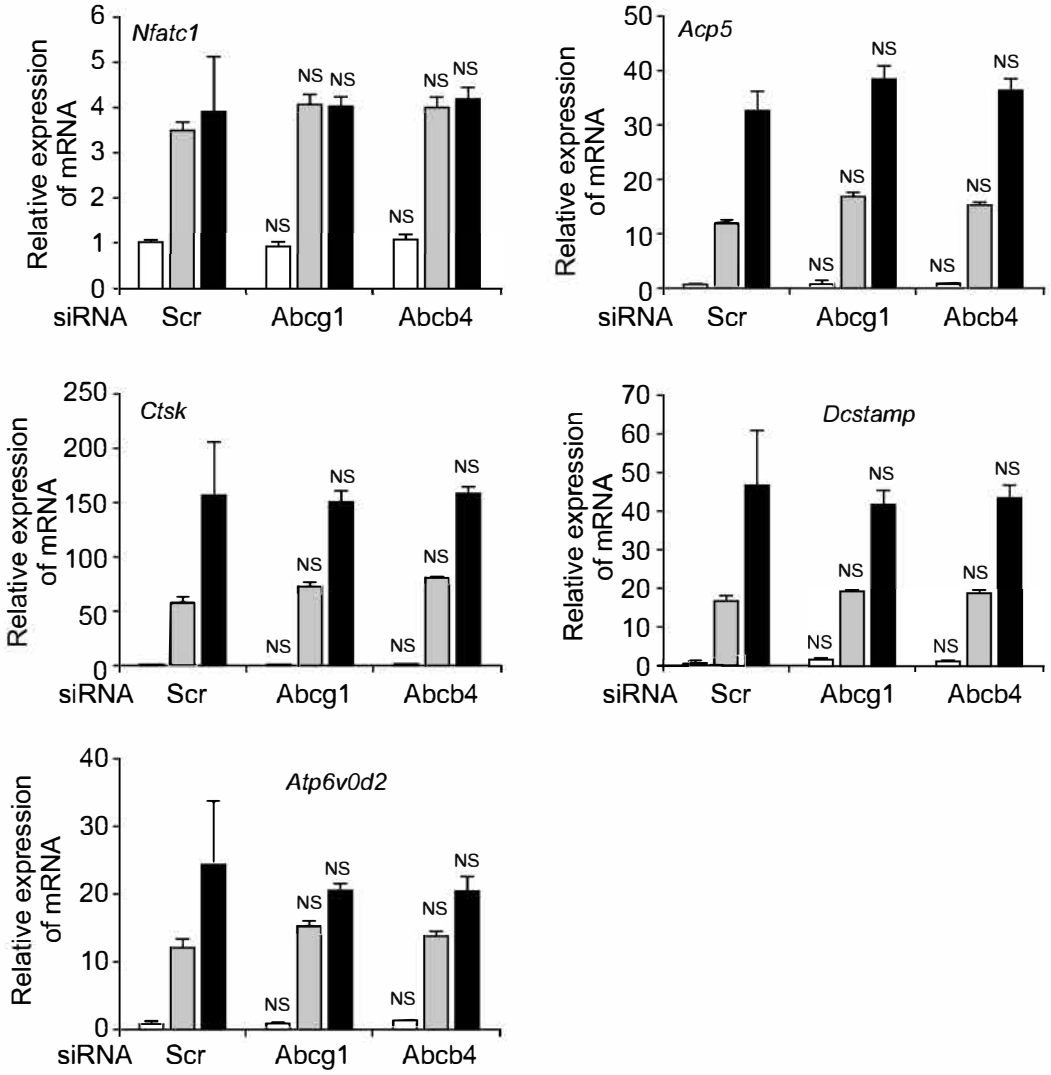

Fig. S5. Effect of *Abcg1* and *Abcb4* mRNA knockdown on mRNA expression of osteoclast-related molecules. WT OCL-precursors were electroporated with scramble RNA (Ser, 1 μM, negative control), *Abcg*1 siRNA (1 μM) or *Abcb4* siRNA (1 μM). After transduction of the siRNAs, the OCL-precursors were cultured with M-CSF and sRANKL. After culturing for one day (open bars), 2 days (gray bars) and 3 days (closed bars), the mRNA levels of *Nfatc1, Acp5, Ctsk, Dcstamp* and *Atp6v0d2* were determined by quantitative real-time RT-PCR. The experiments were performed in triplicate, and reproducibility was confirmed. The values represent the mean ± SD (n = 3). **P* < 0.05 *vs*. culture of osteoclastic cells transduced by scramble RNA on each day. *NS* means that the difference was not significant.

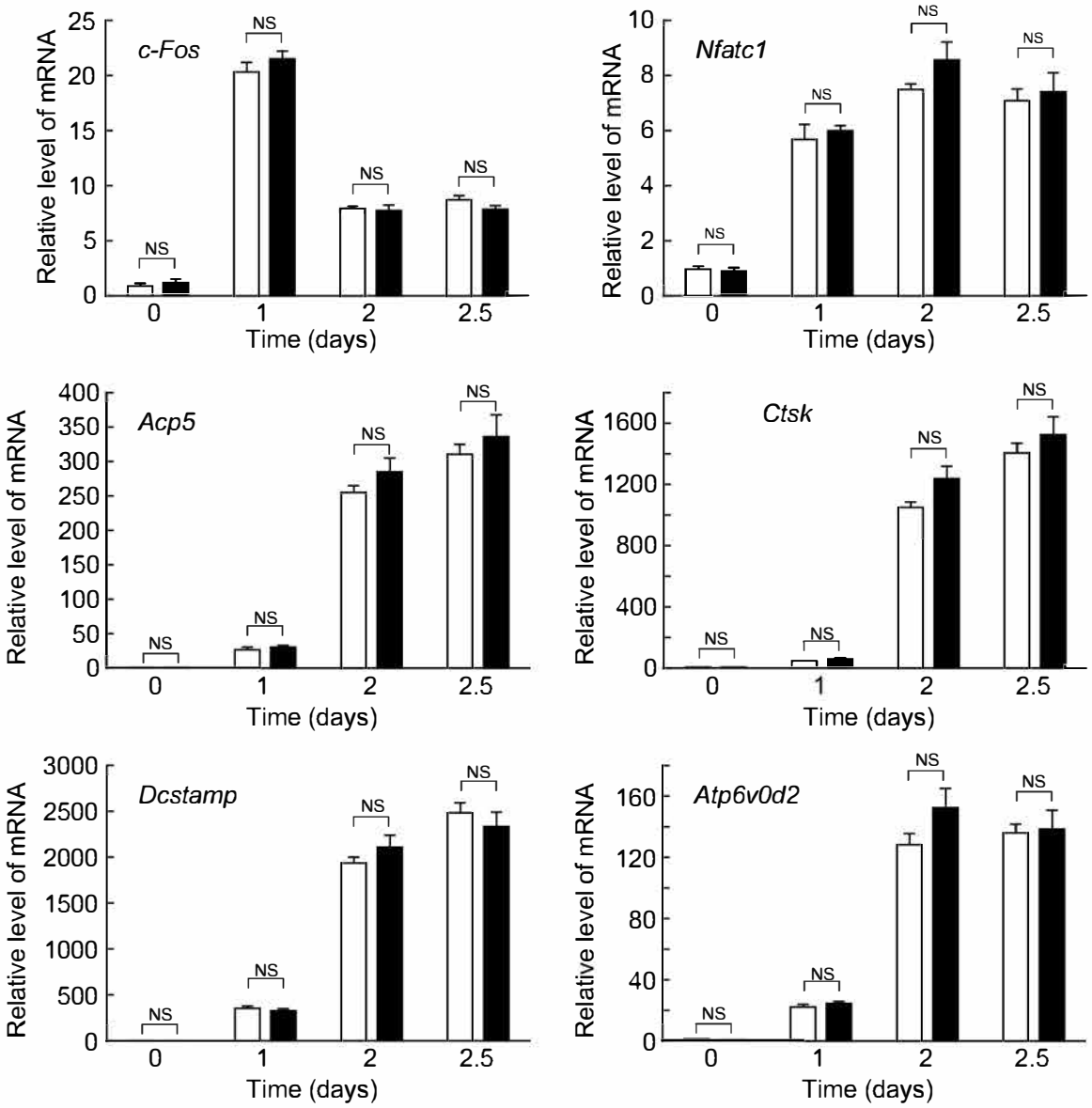

Fig. S6. Exp ession of osteoclast differentiation-related genes in *Abcg1* sKO OCLs. OCL-precursors from WT (open bars) and *ABCG1* sKO (closed bars) bone marrow cells were cultured with sRANKL (10 ng/ml) and M-CSF (20 ng/ml) for the indicated days. After culture, total RNA was prepared, and the synthesized cDNA was subjected to quantitative real-time RT-PCR to determine the mRNA levels of *c-Fos*, *Nfatc1*, *Acp5*, *Dcstamp* and *Atp6v0d2* during osteoclastogenesis. The experiments were performed in triplicate, and reproducibility was confirmed. The values represent the mean ± SD (n = 3). *NS* means that the difference was not significant between the cultures of WT cells and dKO OCLs on each day.

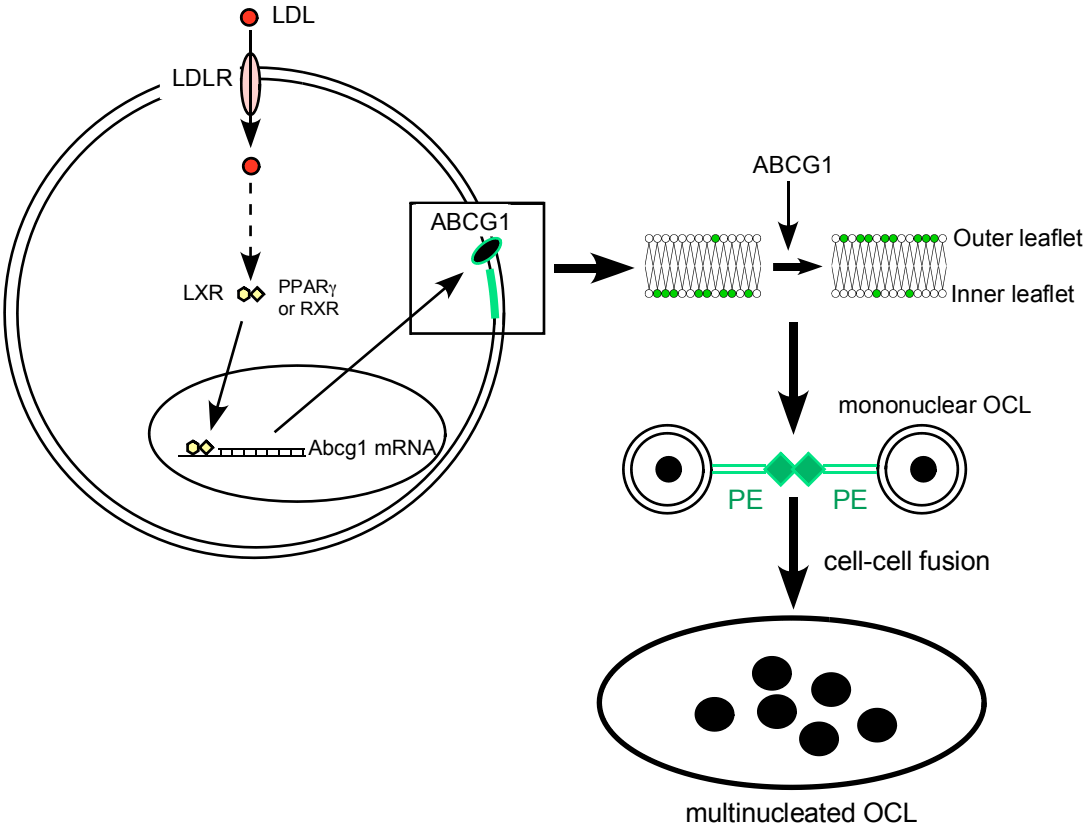

Fig. S7. Scheme of sequential cellular events from LDL-uptake mediated by LDLR up to the cell-cell fusion in osteoclast-like cells *in vitro*.